UNIVERSIDADE DE LISBOA

FACULDADE DE CIÊNCIAS

DEPARTAMENTO DE FÍSICA

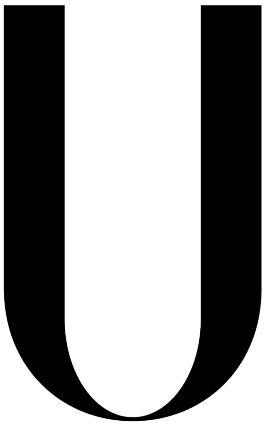

LISBOA

UNIVERSIDADE
DE LISBOA

In vivo dosimetry to narrow down proton range uncertainties

Tiago Mateus Madaleno

Dissertação

Mestrado Integrado em Engenharia Biomédica e Biofísica

Radiações em Diagnóstico e Terapia

UNIVERSITY OF LISBON

FACULTY OF SCIENCES

PHYSICS DEPARTMENT

In vivo dosimetry to narrow down proton range uncertainties

Tiago Mateus Madaleno

Dissertation

Master in Biomedical Engineering and Biophysics

Radiations in Diagnosis and Therapy

Supervisors: Carles Gomà, M. Physicist; Professor Luís Peralta, PhD

2014

Acknowledgements

I would like to express my special gratitude to my supervisor at PSI, Carles Gomà, who introduced me the idea of the project and assisted me during the whole project stages: from sharing ideas and knowledge, planning and executing experiments, to thesis reviewing.

A very special thanks goes out to the Center for Proton Therapy team, particularly to Dr. Albertini Francesca and Prof. Dr. Tony Lomax, who accepted me at PSI as a internship student for this 9 months internship and allowed me to assist to the CPT project meetings and PSI Winter School for Protons, from which I've learnt a diverse issues within the proton therapy field.

My sincere thanks also goes to the Biomedical and Biophysics Engineering professors, who have gave me during my stay at Faculty of Sciences the scientific basis necessary to develop this project. A special thanks to my supervisor Prof. Dr. Luís Peralta, who review and guided me in thesis writing. Additionally, thanks to the responsible persons of Erasmus project, in the person of Prof. Dr. Guiomar Evans, who helped me to apply for it and consequently be accepted.

I must also acknowledge my friends and colleagues I met during this internship, who have shared with me the non-scientific life! More than anyone, they were with me in the best moments.

Foremost, I would like to express my deepest gratitude to my parents, who have truly been following their words: "We don't understand anything about what you are doing, but we trust you".

Abstract

In Vivo exit dosimetry is an approach that has been under investigation as a tool to narrow down the uncertainties associated to proton beam range of dosimetric distributions. The goal of the project is to investigate the feasibility of different dosimeters to minimize the currently established range uncertainty value of ±3%. Measuring the exit dose of certain fields with dosimeters placed in a head phantom surface and compare it with the dose predicted by the treatment planning system (TPS) for the respective dosimetric plan, one can know whether the dose is being overestimated or underestimated. Two cases can happen: if it is experimentally measured a certain amount of dose, the current dosimetric plan calculated by the TPS is being underestimated. Consequently, undershooting scenarios on the phantom can be discarded. On the other hand, if no dose is measured with the dosimeters, overshooting scenarios can be discarded. Five different dosimeters were tested in the head phantom in order to develop a feasible standard procedure for the external *in vivo* dosimetry (EIVD) approach. Two different methods were performed: a first method where TLDs and the ionization chamber (IC) Semiflex (125 mm^3) (from PTW) were placed on the surface of the phantom in 4 different points; and a second method where the 2D array detector (from PTW) was placed perpendicular to the beam, behind the phantom on the opposite side of the gantry nozzle. TLDs, two ICs (Semiflex and Advanced Markus (PTW)) and a diamond detector were placed on the surface of the 2D array over 2 specific points. In the first method two dosimetric plans were measured: a nominal scenario and a overshooting scenario (characterized by a change of +3% in the Hounsfield units (HU) CT), representing the maximum range error possible. Both were used with a clinical field of protons (110º gantry, 180º couch rotation). In the second method, along with the latter scenarios a 10% overshooting scenario was added (HU of the CT changed by +10%) and a experimental field was used (90º gantry, 180º couch rotation). After the necessary results post-processing, the comparison between the measurements obtained experimentally and the respective dose predicted by the TPS (PSIplan) was done. The results show that the dose measured by the dosimeters is not within the ±3% of uncertainty in the range used at Paul Scherrer Intitut (PSI) due to errors inherent to the methods used.

Several approaches were made to overcome this methodological errors, without relevant improvements, however. Therefore, was not found any feasible dosimeter for such EIVD approach.

Resumo

A dosimetria de verificação *in vivo* é uma abordagem que tem sido objeto de estudo como um método para diminuir as incertezas associadas ao alcance de feixes de protões em planos dosimétricos. O objetivo do projeto é investigar a viabilidade da utilização de diferentes dosímetros para minimizar o valor da incerteza atualmente estabelecido de ±3%. Medindo a dose resultante de certos campos de protões que atravessam um fantoma (simulação de uma cabeça humana), com dosímetros colocados na sua superfície, e compará-la com a dose calculada pelo sistema de planeamento dosimétrico para o respectivo plano dosimétrico, é possível saber se a dose está a ser sobrestimada ou subestimada. Dois casos podem acontecer: se for medida experimentalmente uma certa quantidade de dose, o plano dosimétrico calculado pelo sistema de planeamento está subestimado. Consequentemente, cenários com uma distribuição de dose subestimada no fantoma podem ser descartados. Por outro lado, se nenhuma dose é medida com os dosímetros, cenários com a distribuição de dose sobrestimada podem ser colocados de lado. Cinco dosímetros com diferentes características foram testados no fantoma de forma a desenvolver um procedimento padrão viável para a dosimetria externa *in vivo*. Foram realizados dois métodos: no primeiro método TLDs e uma câmara de ionização (IC) (Semiflex (125 mm^3) da PTW) foram colocados na superfície do fantoma em 4 pontos diferentes. No segundo método, um detetor planar ("*2D array*" da PTW) foi colocado perpendicularmente ao feixe, atrás do fantoma, e os TLDs, duas câmaras de ionização (*Semiflex* e *advanced Markus* (PTW)) e um detetor de diamante (*diamond detector*) foram colocados sobre a superfície da *2D array* em 2 pontos específicos. No primeiro método dois planos dosimétricos foram utilizados para as medições: um plano nominal e um plano sobrestimado em 3%, isto é, com as unidades de *Hounsfield* (*HU*) da tomografia computorizada (TAC) alteradas em +3%, representando o erro máximo possível no alcance. Ambos foram usadas com um campo clínico de protões (110º rotação da *gantry*, 180º rotação da mesa). No segundo método, juntamente com os últimos planos, um plano sobrestimado em 10% foi adicionado (*HU* da TAC alteradas em + 10%) e um campo experimental de protões foi utilizado (90º rotação da *gantry*, 180º rotação da mesa). Depois do processamento dos resultados necessário, foi efetuada a

comparação entre as medições obtidas experimentalmente e a dose respetiva prevista pelo sistema de planeamento (*PSIplan*). Os resultados mostram que a dose medida pelos dosímetros não está dentro da incerteza no alcance utilizada no Paul Scherrer instituto (*PSI)* devido a erros inerentes aos métodos utilizados. Várias abordagens foram feitas para contornar estes erros metodológicos, no entanto sem melhorias relevantes. Não foi portanto encontrado nenhum dosímetro viável para o método de dosimetria externa *in vivo* proposto.

Contents

1. Introduction **1**

1.1. Paul Scherrer Institut - Center for Proton Therapy **3**

1.2. Objectives **3**

1.3. State of art **4**

2. Fundamental concepts **7**

2.1. Physics **7**

2.1.1. Protons interaction in matter 7

2.1.1.1. Stopping power 7

2.1.1.2. Multiple Coulomb scattering 8

2.1.1.3. Nuclear interactions 8

2.1.2. Fundamental physical quantities 9

2.1.3. Depth dose distribution - Bragg peak 10

2.2. Proton therapy techniques **11**

2.2.1. Passive scattering: the spread-out Bragg peak 11

2.2.2. Active scanning 12

2.3. Proton dose distributions **13**

2.3.1. SFUD and IMPT 14

2.4. Proton therapy at PSI - CPT facility **14**

2.5. Range uncertainties **17**

2.6. CT HU to relative stopping power **18**

3. Materials and Methods **21**

3.1. Experimental procedure **21**

3.1.1. Overshooting scenarios development 21

3.1.2. Dosimetric plans 24

3.1.3. Method 1 - Detector on the surface of the skin 25

3.1.4. Method 2 - 2D array approach 26

3.1.5. Dosimeters 28

3.1.5.1. Thermoluminescent dosimeter (TLD) 28

3.1.5.2. Ionization Chambers 28

3.1.5.3. Synthetic Single Crystal Diamond Detector (SCDD) 29

3.1.5.4. 2D detector array 30

3.1.5.5. Characterization of non-standard dosimeters 31

3.1.5.6. Dosimeters global evaluation 33

3.2. Analysis procedure **34**

3.2.1. Robustness plan tool 34

3.2.2. Method 1 - Detector on the surface of the skin 35

3.2.3. Method 2 - 2D array approach 36

3.2.3.1. Simulation of the 2D array entrance window 36

4. Results **39**

4.1. Method 1 - Detectors on the surface of the skin **39**

4.1.1. Results 39

4.1.2. Discussion 41

4.2. Method 2 - 2D array approach **41**

4.2.1. 2D array 42

4.2.1.1. Post-processing of the TPS dose distribution 42

4.2.1.2. Results 43

4.2.1.3. Discussion 46

4.2.2. Point detectors over the 2D array 46

4.2.2.1. Discussion 48

5. Conclusion **49**

6. Bibliography **53**

1. Introduction

Nowadays, it is a known reality that cancer is among the main causes of death worldwide. In 2012 it was registered about 8.2 million of cancer deaths. Due to the advances of the medical knowledge and the high evolution of the intersection of technology with medicine in the past decades, the death cases have been decreasing, however, it is expected a rise of the annual cancer cases from 14 million, in 2012, to 22 million within the next two decades [1]. These numbers reflect the importance of research and investment in new medical techniques and essentially the reinforcement of the well established technology.

Cancer can be generally treated by one or more selection of medical interventions such as: surgery, chemotherapy and radiotherapy. Each one of these medical modalities are vast and characterized by an extensive set of techniques emerged from the intersection of the knowledge between different scientific fields. Unquestionably, radiotherapy owes its existence to this interchange, specifically to the evolution of technology driven by the Engineering and Physics fields. Therefore, radiotherapy is object of study within Biomedical Engineering including thus the relation with these transversal scientific areas. This thesis contemplates the study and research of a current issue within proton therapy, which is one of the particle therapies that constitute the external radiotherapy field.

The main challenge as well as the goal of external radiotherapy is to deliver a certain prescribed amount of dose to the treatment tumor volume by means of ionizing radiation, whilst sparing the surrounding healthy tissue as much as possible. Since the radiation source is located outside the patient, the radiation will always transverse the healthy tissue to reach the tumor and deposit energy on it. Although the technical impossibility to completely spare it, one can obtain clinical acceptable treatment plans according the treatment characteristics implemented such as: the ionizing radiation employed; the clinical case involved (for instance the localization of the tumor), the correspondent delivery treatment technique (the position and number of fields for instance) and the inherent optimization technique (in conventional radiotherapy for instance, whether it is used IMPT or not).

External radiotherapy is performed with different kind of particles. The so called conventional radiotherapy uses photons and electrons and is by far the most worldwide available technique, since the costs involved to create the necessary technology are much lower. Additionally protons are also used and in a much lesser extent, heavy ions like carbon ions. They are called respectively, proton therapy and heavy-ion therapy.

Regarding the protons, their physical characteristics of interaction with matter have a big potential. Specifically, the integral dose along the path of the protons, when interacting with matter, shows a sharp peak (Bragg-peak) followed by a steep fall-off region. This steep dose gradient at the distal edge of the Bragg peak is consequently translated in a well-defined finite range. The exploitation of this physical property through the techniques available nowadays, result in a treatment with a lower integral dose to the patient and a dose deposition highly localized in the target when using proton therapy rather than conventional radiotherapy. Therefore, theoretically, there is a gain in the therapeutic ratio1. Maintaining the target prescribed dose, it is also verified, roughly, a reduction of the total energy deposited when treating a tumor by a factor of three, when compared with conformal photon radiotherapy, and by a factor of two when compared with intensity modulated radiotherapy (IMRT) [2, 3].

However, these same physical characteristics also make the calculation of the exact range and localization of the beam an important issue to be considered, otherwise they can likely induce a clinically unwanted impact on the predicted treatment [2, 4]. In practice, an underestimation of the range might cause an over-dosage of healthy tissue, i.e. a clinical overshooting treatment, whereas an overestimation might lead to an under-dosage of the whole tumor volume and to a clinical undershooting treatment.

These uncertainties of a proton beam come from multiple sources and they are the main factor which actually limit the fully exploitation of the proton therapy potential. In fact, if this issue is overcome or at least minimized, several clinical cases which are nowadays performed using photon therapy treatments could be improved significantly through proton therapy treatments. For instance, in prostate cancer treatments using radiation therapy, the finite range of proton beams could be used as a tool to create an anterior single field plan, shielding critical structures (such as the rectum) with shorter path lengths through healthy tissue. However, the standard treatments of prostate cancer employ proton parallel-opposed lateral beams or advanced forms of conventional radiotherapy (such as intensity-modulated radiotherapy (IMRT)), just because this method is more robust to proton beam uncertainties, despite increasing the volume of healthy tissue irradiation [5].

These range uncertainties and the way to deal with them are indeed a relevant issue in proton therapy and has been an important topic of investigation within the research community. The later

1 The therapeutic ratio is defined as the ratio between the probabilities for tumor eradication and normal tissue complication

example shows the importance of being able to monitor the range of the proton beams in vivo. This thesis is focused then in trying to find a way of measuring the dose in vivo, out of the patient, since it can be directly a relevant tool to evaluate and decrease the uncertainty in the range. In vivo dosimetry in external radiotherapy has already been a clinical solution to deal with this issue and, undoubtedly, an important research topic within proton therapy breakthroughs [6].

1.1. Paul Scherrer Institut - Center for Proton Therapy

This thesis is a result of a internship project elaborated at Paul Scherrer Institut (PSI), in Switzerland. PSI is actually the main research center for natural and engineering sciences within Switzerland. It focuses on the long-term research in three different areas: Matter and Material, Energy and Environment and Human Health. The Center for Proton Therapy (CPT) has been treating patients since 1984, when it was installed an horizontal beam line to treat ocular melanomas. Since 1996 the first proton therapy gantry developed in-house has been in operation and in November 2013 the new Gantry 2 began treating patients with more advanced techniques. Never ceasing to be a leader in research and development (R&D), CPT started in fact treating patients as a year-round facility in 2007, when the new dedicated cyclotron for medical purposes was lunched. A new gantry (Gantry 3) is being under construction, with the same treatment capabilities of Gantry 2, and is planned to be lunched in 2016 [7].

1.2. Objectives

The finite range of protons is one of the major advantages which led to the development of proton therapy. The way to overcome its inherent uncertainty however, is actually one of the foremost research topics not only at PSI but also in the world proton therapy community. This thesis is a result of an experimental project which was held in CPT at PSI, and follows the development pathway of robustness in treatment planning techniques that has been carrying out in CPT R&D program. It focuses on the feasibility of using point dosimeters to verify the range of the beam in order to narrow down as much as possible its uncertainties.

The motivation of the project arises because it was verified in some exceptional cases, with a superficial target, that the protons can go through the patient and deposit a considerable amount of dose in a healthy tissue. In the example of a patient plan approved for treatment displayed in the figure 1, this is the case, where one can find doses between 20% and 90% of the prescribed dose in the healthy tissue located in the exit region of the beam, out of the target.

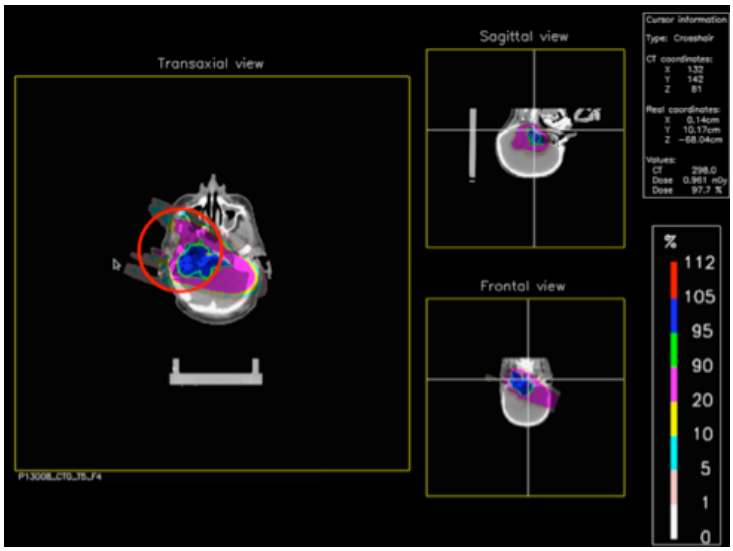

Figure 1: Clinical plan treatment performed at PSI. It is clear that there are still dose between 20% and 90% of the dose prescribed in the healthy tissue located in exit region of the beam

The main aim of the project is then measure with different point dosimeters the dose delivered by a proton beam on the surface of the skin, in the distal edge of the target. The experiments are performed on a head phantom existent at CPT specifically made for proton therapy research experiments. Two results can be obtained: either it is measured some dose, meaning the range is being underestimated by the TPS and undershooting scenarios no longer are taken into account; or it is not measured any dose and overshooting scenarios can be discarded. Therefore, the result will always be automatically useful whether is measured dose or not. Depending on the relevance of the results obtained, setting up a standard procedure to test this external *in vivo* dosimetry approach (EIVD) is also a goal.

1.3. State of art

In conventional radiotherapy, *in vivo* dosimetry has been a simple and accurate safety tool to avoid dose delivery errors during specific treatments and a wide range of EIVD techniques have been developed [6]. Due to the high sensitivity of proton therapy delivery calculations to range errors these EIVD approaches are for sure an asset.

Regarding the direct methods of *in vivo* range verification, Mumot et al (2010) proposed the concept of 'range probe', i.e. a proton pencil beam with low-dose but high-energy which penetrates through the patient where a multi-detector would measure the integral Bragg peak dose. Such measurement would be compared with the one calculated by the TPS so that the accuracy of the range *in vivo* could be evaluated. Based on Monte Carlo simulations it appears feasible that range errors in the order of 1 millimeter could be detected [8]. This approach is simple, requiring only a commercial

multi-layer ionization chamber (MLIC) detector, however, it requires high energy protons (around 250 MeV), depositing unnecessary dose at the patient; shows a low resolution and is not able to measure the range directly at the exit of the tumor position, only the range through the whole patient body [2]. In order to improve the range verification of point based dosimetry Lu et al (2008) explore the properties of range modulated passive scattering fields, more precisely the fact that at any point of the target, the time dependence of a spread out Bragg peak (SOBP) distribution is unique. So measuring with a point dosimeter this time dependence of the dose rate one is able to determine the depth information and then the residual range of the beam can be predicted with millimeter accuracy [9]. This approach is however limited to this delivery system (SOBP). Additionally, the dosimeters must be placed close or within the target volume, which is not always possible and is invasive for the patient. Besides, these tests were performed in an homogeneous water phantom environment and this approach remains to be validated either in heterogeneous body phantoms or in real clinical situations [2]. The accuracy of the implanted markers methods will be extremely dependent of the heterogeneity effects of the patient body structure but indeed a real conclusion about the accuracy remains to be investigated in those circumstances.

Apart from point dosimetry, 2D tools for in vivo dose measurements have been as well developed. Proton radiography is a technique which requires high energy protons applied to the patient [10]. Beyond the advantages of proton radiography against x-ray radiography, in this context, the use of this approach is justified by the fact that it directly provides the tissue stopping power values. Therefore, the uncertainties would be minimized since the computer tomography (CT) Hounsfield units (HU) to stopping power calibration as well as it inherent uncertainties would not be anymore presented within proton therapy technique [2]. Despite these clear advantages proton radiography has not progressed rapidly and clinical implementation is still a distant expectation.

Besides the latter approaches there are as well other methods able to verify the proton range *in vivo* in an indirect way. Along the proton path, inelastic interactions with the target nuclei occur, leading to its excitation to a higher energy state and consequently emitting a single photon (prompt gammas) to return to its ground state. The direct employment of this radiation for range verification was first proposed by Min et al. They suggest that the correlation of high energy prompt gamma rays with the penetration path of protons in the tissue can be used to indirectly verify the proton range. Although the prompt gamma fall-off is not equal to the proton fall-off a consistent and predictable fall-off differences allow the proton range verification [11]. Currently the application has failed because has not been developed so far a optimized prompt gamma detector, however, considering recent developments, sub-millimeter precision in range measurements seem to be feasible [12]. Moreover, with this approach the range verification is able to be performed in real time and without additional dose [2].

The use of positron emission tomography (PET) as a tool to verify the proton range was firstly investigated by several groups world wide in the 90's [13-16] but continues under development both for protons and heavier ions. The method is based on the detection of beta$^+$ activity which is formed by inelastic collisions between protons and elements in tissue. Specifically, the inelastic nuclear reaction cross sections tend to occur at higher energies along most of the beam flat path and decrease at the Bragg peak zone i.e there are a diminish of the positron emitters concentration [17]. Analyzing PET image it shows beta+ activity up to the Bragg peak and then falls off. Therefore, comparing the measured distributions by PET with predictions based on the treatment plan, it is possible an effective range verification. This approach could be used both off-line, with a little delay after the treatment in a commercial PET scanner, or on-line, directly following the treatment with a facility specific detector solution. For the latter only 3 clinical installation exist and several technical improvements are required. In general the accuracy of the range verification is around 5-10 mm [18].

Finally, *in vivo* dose verification using magnetic resonance imaging (MRI) has been reported in several studies among which the work of Gensheimer et al stands out. One of the consequences of ionizing radiation is that it can cause alterations in the human tissue which are able to be detected by MRI [19]. This is hence a off-line method with high spatial resolution and no additional ionizing radiation. Nevertheless, a visual evaluation is not sufficient to verify the proton range because the location of the greatest signal intensity (SI) does not correspond necessarily to the delivery dose gradient. The relation dose-SI is not linear and is not well established but if such relation could be found, sub-millimeter precision is conceivable. The low temporal evolution of the MR signal (about 8 days was reported) is still as well an disadvantage [2].

2. Fundamental concepts

Proton therapy is an external radiotherapy modality which uses protons to delivery the required dose distribution for a given target in a patient in order to treat a patient with cancer. Between the proton acceleration until the end of beam delivery system, there are many and complex engineering techniques developed during the later decades integrated in this therapy method. Apart from that, there are implicit in these techniques a vast amount of physics concepts. Therefore this chapter contemplates the main concepts and techniques that had a direct relation with the development of the project and enable the understanding of the results.

2.1. Physics

2.1.1. Protons interaction in matter

The most important interactions of particles with the matter are actually well defined by physics models. Each particle, depending on their fundamental characteristics such as size or charge, shows a different way of interaction. The characteristics of the therapy performed is then closely related with the particle used. Specifically for the purpose of the project, understand how protons interact with tissue is fundamental.

2.1.1.1. Stopping power

When protons go through the matter they are subjected to electromagnetic Coulomb interactions with the orbiting electrons of atoms resulting in continuous loss of energy. These interactions lead to the ionization and excitation of atoms and set free electrons that ionize other atoms in the neighborhood. Although the protons lose little energy and almost no deflection in these individual interactions, they experience thousands of interactions per centimeter [20]. The rate at which they lose energy, transferring it to the tissue, increases with the penetration depth and is described by the mass

stopping power. For protons, which have mass higher than electrons, the stopping power is described by the Bethe-Bloch equation [3]:

$$\frac{S(E)}{\rho} = -\frac{1}{\rho}\frac{dE}{dx} = 0{,}3072\frac{Z}{A}\frac{1}{\beta^2}\left(\ln\frac{T_{\max}}{I} - \beta^2\right), \tag{2.1}$$

in MeV·cm2/g as SI unit. Concerning the parameters relative to the medium, ρ is the density, Z and A are respectively the atomic and nuclear number and I the mean excitation energy. The latter one can not be calculated with relatively good accuracy so it is inevitable a cause of uncertainty in the proton range. On the other hand Tmax is the maximum proton energy transferred to a free electron in a single collision and is given by:

$$T_{\max} = \frac{2m_e c^2\beta^2}{1-\beta^2}, \tag{2.2}$$

where me is the electron mass, c the velocity of the light and β is a kinematic term equal to v/c. The examination of the Bethe-Bloch equation reveals the approximate proportionality: S(E)∝1/v2, for low energy protons [2, 3]. The smaller the velocity of the protons, the higher the energy loss.

2.1.1.2. Multiple Coulomb scattering

Protons are also scattered by the atomic nucleus, resulting in an angular deflection of their path. Despite they experience also a slightly deflection due to electrons of the atoms of the matter, this is almost irrelevant, since the protons are 1800 times heavier. Consequently this effect is ignored in some mathematical models without relevant consequences [2]. On the other hand, when a proton passes close to an atom nuclei, which is heavier than an electron, suffers an repulsive electrostatic force resulted from the positive charge of the nucleus. This interaction leads to a small but relevant deflection in the proton path. Along its path the proton suffers many small deflections which add up to a statistical significant angular deviation. The resultant scattering is named Multiple Coulomb scattering (MCS) [2, 20].

2.1.1.3. Nuclear interactions

Together with the Coulomb interactions with the electrons and nuclei, primary protons have a small probability of suffering elastic and nonelastic nuclear interactions. In elastic nuclear collisions, the proton is deflected by several degrees but the nuclei maintains intact and kinetic energy is conserved. On the other hand, and more important, in nonelastic collisions the nuclei may breakup, changing its initial characteristics, and secondary particles such as secondary protons, neutrons, γ rays,

heavy fragments (alpha particles) are emitted. After the interaction the primary proton is then widely deflected and loses a significant part of its initial energy. The secondary particles have in general much lower energy and larger scatter angles than the incident primary proton. Around 1% of protons per centimeter are lost from the beam due to nonelastic interactions [2, 3].

These nonelastic interactions are difficult to model, either analytical or using Monte Carlo simulations, however, since their biological effect is considerable small they are taken into account in the beam design by using measured experimental Bragg peaks [3].

2.1.2. Fundamental physical quantities

In the radiation physics field, and in the context of the project, there are some physical quantities that must be defined. The proton therapy treatments uses then the energy deposited by the proton beams to destroy the tumors. In radiotherapy, the quantity absorbed dose is the measurable standard for the amount of ionizing radiation in a medium, particularly a tissue, and it is defined as the mean energy absorbed per unit mass:

$$D = \frac{d\bar{E}}{dm}, \tag{2.3}$$

The SI unit of dose used in radiotherapy is the Gray (Gy), which corresponds to J/kg [3, 21, 22].

The damage of the radiation can be thus evaluated as a function of dose, i.e, there are a dose-response relationship, however, this biological effect depend as well on the radiation. Protons, for instance, are more biologically effective than photons meaning that is necessary lower dose when using protons to reach the same biological effect. To evaluate this effect the relative biological effectiveness (RBE) value, which uses the x-rays as reference, is defined:

$$RBE = \frac{D_x}{D}, \tag{2.4}$$

where D corresponds to the value of a certain radiation dose which lead to a specific biological effect while D_x is the x-ray dose necessary to produce the same effect [3, 21]. In order to maintain the consistency in the clinical and due to the large quantity of clinical results with photon beams available, the dose is prescribed as photon doses regardless of the type of radiation [3]. However, the dose can still be evaluated taking into account the RBE, simply dividing the photon dose by the RBE value.

Regarding proton therapy, the value of *RBE* for protons is 1.1, a value calculated with animal experiments in the earlier days. Despite this parameter has a dependency on different physical and

biological parameters it is used as a constant value. In fact there are no clinical indication that 1.1 can lead to unexpected results and side effects and a generic value allow a straightforward conversion from photon doses into proton doses of clinical treatments [3].

2.1.3. Depth dose distribution - Bragg peak

The physical interactions referred above result in a dose to the tissue along the protons path. This dose distribution of the protons in depth shows a peak, representing a large increasing of dose just before the protons stop, resulting from the increasing of the stopping power as the protons slow down. This depth dose curve is named Bragg peak and contrasts with the short dose build-up followed by a exponential-like decay of the photons dose distribution (figure 2). This characteristic is the basis of proton therapy. In fact the techniques of proton therapy are essentially different ways to manipulate this Bragg peak in order to optimize the treatment: covering the target and sparing the healthy tissues as far as possible [3].

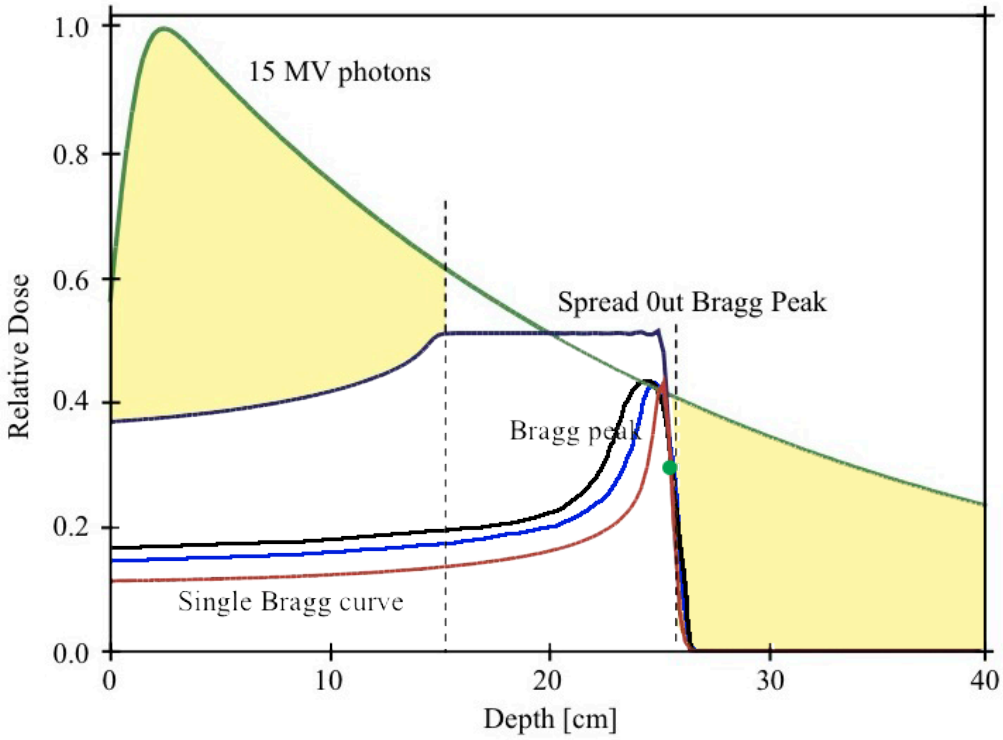

Figure 2: Representation of the depth dose curve (Bragg curve) and spread-out Bragg peak (SOBP) of protons compared to the depth dose curve of a 15 MV photon beam. The yellow area indicates the amount of dose that can be avoided by using protons instead of photons for a tumor positioned between the two dashed lines. The black, blue and red Bragg peaks represent 3 different energy spreads with the same mean energy. The green dot is the dose at the distal 80% peak which corresponds to the point with the same depth regardless of the energy spread (adapted from **[39]**).

The Bragg peak shape is also consequence of the energy spread and the range straggling. Energy spread is a characteristic of any clinical proton beam since its technically impossible to create a mono-energetic beam. A clinical proton beam actually consists of a small spectrum of energies with a certain mean energy. Since the energy of the proton beam is the property that defines the depth, this energy spread causes then a difference on the depth of which the protons stop. Additionally, for each of this small spectrum of energies there is a range straggling. This concept means that even in a mono-energetic beam the protons do not stop at the same depth. In fact the energy loss, which is a process caused by a large but finite number of interactions, has inevitably inherent a statistical fluctuation. [3]. These interactions together define the width of the Bragg peak and the slope of the steep fall of region.

The proton range is then quantitatively defined taking into account these properties of the Bragg peak. Depth dose measurements show that if one increase the energy spread of a proton beam with a certain mean energy, the distal 80% point of the peak remains the same (figure 2). The depth at this correspondent point is then considered the range of a proton beam [3].

2.2. Proton therapy techniques

A unmodified proton beam - often named as pencil beam - that is extracted and transported from an accelerator, has dimensions on the order of millimeters and a narrow energy spectrum, as referred above. However the dimensions of the clinical target are in general larger than the proton beam and with different shapes. Therefore it is necessary to spread out the beam in three dimensions in order to cover the entire volume of the target with the required dose.

There are different deliver techniques in proton therapy created to manipulate the proton beam and are divided into two modes: passive scattering and active scanning. The first mode is currently the most mature and used worldwide and apply mechanical instruments to spread out and create a broad beam suitable for therapy. The second one comprises the use of several techniques in order to handle the position of a single pencil beam across all the volume of the target.

At PSI passive scanning is only used in the horizontal beam line at OPTIS 2. On the other hand both Gantry 1 and Gantry 2 perform active scanning, despite using different techniques.

2.2.1. Passive scattering: the spread-out Bragg peak

Passive scattering uses scattering and range shifters materials to scatter the beam laterally and in depth, respectively (figure 3a). These components are placed in the nozzle, the head of the gantry. There are actually different approaches to broaden the beam using different scatter foils. Generally a first flat scatterer is used to scatter the beam uniformly to a second scatterer with variable thickness, which scatters the beam more in the center than close to the edges. This composition flattens out the

lateral profile of the initial beam, which is a Gaussian with a spread of about 1 centimeter [3, 20, 23]. In order to conform the beam laterally is used an aperture which serves as well as collimator. The shape of the aperture is defined according to the shape of the target, with margins made usually of brass that collimates the beam, preventing the healthy tissue next to the target of receiving dose. This component should be placed close to the patient so then the penumbra could be minimized [3, 20].

Along with the lateral conformation it is also necessary a depth conformation of dose. As explained before the depth dose curve of a pencil beam is a Bragg peak, characterized by a high variability of dose deposition in depth. To obtain thus a homogenous dose distribution over the target volume it was found out that a superposition of many Bragg peaks with a specific energy and weight would fulfill this goal. This homogenous extension in depth is named spread-out Bragg peak (SOBP) (figure 2). To practically achieve that it is used a range modulator device such as a range modulation wheel or a ridge filter. The first one is the most commonly used and consists of a wheel with steps of varying thickness which is irradiated while the wheel rotates. The thickness of each step determines the range shift of the Bragg peak and the angular width determines the weight of that Bragg peak [3]. Compensators are as well used. They define the shape of the distal edge of the proton beam in order to make it coincide with the distal surface of the target. This is accomplished adding more material to the compensator in the beam direction, where the the depth is small, and less material where larger beam penetration is desired [3, 20].

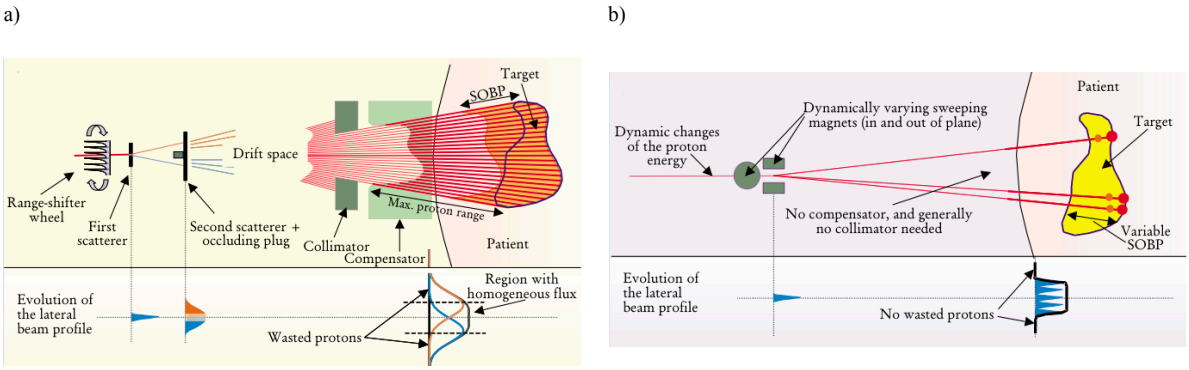

Figure 3: a) Representation of a standard passive scattering system. First a range modulator system (range shifter or a modulation wheel), two scatterer foils (a flat scatterer and second scatterer with variable thickness), a collimator (aperture) and a compensator. Is it visible that the SOBP has always the same width along the beam direction, delivering then the prescribed dose also to the healthy tissue proximal to the target. Below in the same image is represented the evolution of the lateral beam profile along the beam path. b) Representation of a standard active scanning system. A dynamic device which allows the definition of the proton energy (range shifter or a degrader, for instance) and scanning magnets which allow the dynamic change of the beam position. Below the evolution of the lateral beam profile is also shown (adapted from **[23]**).

2.2.2. Active scanning

Active scanning is a method where a narrow proton beam is applied to scan the target both laterally and in depth. This can be applied by either magnetic or mechanical modes, or by the

combination of the two, and requires a sophisticated control system technology in order to perform a secure and accurate treatment (figure 3b) [20]. Active scanning nowadays is mostly performed through the spot scanning technique, where the dose is delivered in small steps. Specifically, a pre-determined dose is delivered to a certain spot, then the beam is switched off, the magnetic setting are changed to target other spot, the dose is delivered to this new spot position, and so forth. Raster scanning is as well used, mainly for heavy ions, and is similar with the spot scanning technique, but the beam is not switched off. It is applied instead a continuous scanning of the target [3]. As well as passive scanning, active scanning techniques differ between facilities, depending on the specification of the research program or depending on the equipment supplier. Although, to perform active scanning the main components are similar.

Protons are charged particles which, when subjected to a magnetic field, are deflected. This property is the basis to use scanning magnets (sweeper magnets) to control the lateral (transversal and longitudinal) position of the beam, instead of using a scatterer system to broaden the beam [24]. Typically the beam is scanned in a zigzag pattern in the plane perpendicular to the beam direction, starting in the deepest layer. To move the beam along its axis to another layer and change the range of the proton beam, it is necessary to change its energy. This is done through the same method used in passive scattering, using a range modulation wheel or a ridge filter.

Active scanning has some advantages over the passive scattering method. There is no need of scatterers and patient specific hardware in the beam way, which are made of materials with large cross section for neutron production such as the aperture, placed moreover close to the patient. Additionally these components are responsible for a loss of around 50% of protons, making active scanning much more efficient. The dose conformity obtained using active scanning is better, since it can create any physical possible dose distribution [20]. However, the majority of facilities worldwide still uses passive scattering since it is a robustness technique; the nozzle components just need to be in the correct path in order to obtain the correct dose, whilst with scanning it is necessary a sophisticated beam control and feedback systems [3].

2.3. Proton dose distributions

As explained, with passive scattering the target can be fully covered using the SOBP characteristics; allowing a dose distribution similar with the one obtained with conventional radiotherapy. One of the main limitations of the SOBP technique is its fixed length. The range modulation system defines the width of the SOBP along the beam direction, which is invariable across the field width, and can not be changed during a treatment field unless it would be possible to change the range modulation system. Since the target volume has a variable thickness along the beam direction, there are then some proximal healthy tissue irradiated with the full dose (figure 3a). In spite

of being possible to create a SOBP with active scanning, the goal is to create a variable effective depth dose curve across the width of the field in order to achieve a better dose conformation and spare the healthy tissue.

2.3.1. SFUD and IMPT

At PSI two active scanning delivery techniques are implemented in both gantries and can be used for clinical treatments. Single field uniform dose (SFUD) is a dose delivery technique equivalent to the SOBP dose distribution obtained with passive scattering. However, only the Bragg peaks within the target volume are delivered and the weight (fluency) of each individual Bragg peak is optimized and modulated [24]. This optimization is performed per field individually in order to create a more or less homogeneous dose distribution (within ±10% of the prescription dose). Unless for specific treatments such as ocular melanomas, the SFUD treatments are performed commonly as a contribution of several optimized fields in order to improve the homogeneity of the dose distribution and the robustness of the treatment. In the context of the project thesis, all the dosimetric plans created were calculated and performed with the SFUD technique [3].

Active scanning actually stands out by the possibility of delivering intensity modulated proton therapy (IMPT), the proton therapy equivalent to IMRT. The major and relevant difference between IMPT and SFUD is the optimization process. Rather than optimizing each individual field, the optimization process of IMPT takes into account all the fields used in the dosimetric plan. The fluency of all dosimetric plan Bragg peaks selected within the target volume are optimized simultaneously, regardless of the field to which they belong. Therefore, the homogeneity of the dosimetric plan is just achieved as the result of the sum of all individual fields since the homogeneity per field is not a required parameter. IMPT increases the flexibility of the dosimetric planning and consequently improves the dose conformity to the target, minimizing the dose to the healthy tissue [3, 24]. Specifically, for instance, the weight of pencil beams passing through some critical organ at risk (OAR) could be reduced and compensated by the pencil beams of other fields. The major drawback of IMPT is that the plan robustness is compromised since the single field distribution are extremely complex and irregular [3].

2.4. Proton therapy at PSI - CPT facility

Proton therapy is a modality of radiotherapy which requires complex, large size equipments inside a large facility. Nowadays a proton facility is divided into three main parts: an accelerator, a beam transport system and a treatment delivery system. Each one of the equipments are configured and selected according to the delivery techniques used and the patient tumor location. Usually, for an efficient use of the beam, one accelerator is the source for several treatment delivery systems [20]. The

PSI CPT facility is not an exception: it consists of an accelerator serving two treatment rooms with a gantry each and a third room with a horizontal beam line (figure 4) [7].

a) b)

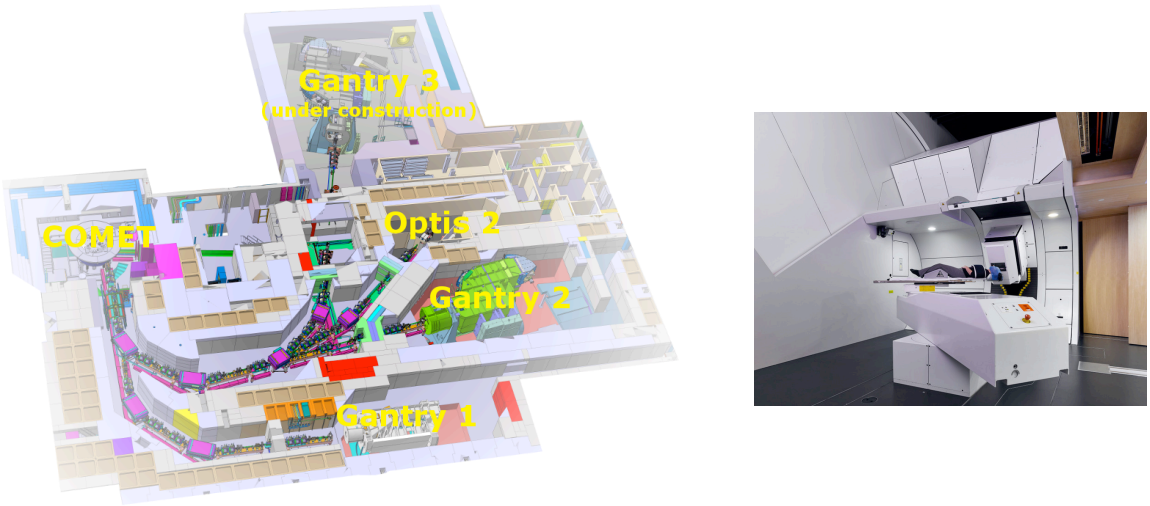

Figure 4: a) Layout of the CPT facility. The COMET accelerator serves 4 treatment rooms: Gantry 1 and Gantry 2 treatment rooms; Optis 2 treatment room with an horizontal beam line and Gantry 3 treatment room, which is under construction to date. b) Image of the Gantry 2 treatment room where were performed the experimental measurements (adapted from **[7]**).

There are two specialized accelerators used in proton therapy: the synchrotron and the cyclotron. The synchrotrons main advantage is that they allow the extraction of protons when it reaches the desire energy, but they have larger dimensions than the cyclotrons. These latter ones are smaller but they produce protons with a fixed energy. The variation of the energy must be then done downstream on the beam line using fast degraders, i.e., inserting a variable amount of material in the beam line [3, 20]. At CPT it was installed a more compact superconducting cyclotron which accelerates protons to a fixed energy of 250 MeV. This accelerator type was chosen since the way of energy selection associated to it allows the development of more performing scanning techniques such as specific techniques for moving targets. At Gantry 2 for instance, along with a range shifter a degrader was installed upstream in the beam line (figure 5). The energy changes with a high rate, in small steps very quickly (takes around 100-150 ms), whilst in a synchrotron it is necessary to wait for the next pulse of acceleration [25]. On the other hand, this method of reducing the energy also deteriorates the quality of beam and brings some safety issues that must be corrected. [25].

Proton beams reach the treatment delivery system guided and focused by magnetic structures in the beam line. Rotational gantries are the most used treatment delivery system in proton centers, however, as referred above, for special tumors like ocular melanomas a horizontal beam line is preferred. Proton therapy gantries were created essentially to allow the beam to be directed towards the patient from any direction of the vertical plan of rotation. In Gantry 2 nozzle for instance, two

sweeper magnets control the lateral position of the pencil beam, which then is deflected by a 90ª bending magnet. Together with a couch which can have six degrees of freedom it is possible to achieve many beam directions [26].

Another important characteristic of gantries is that its spatial positions and the position of the patient must be extremely reproducible because the tumors are always located close to the healthy tissue. Additionally, a high position stability and shape invariance of the beam must be provided at all gantry rotation angles in order to achieve a high beam-pointing accuracy. Gantries are actually a technically complex structures since they are equipments with a huge size and a weight of about 100 tons that must be controlled with a sub-millimeter mechanical precision [20, 25].

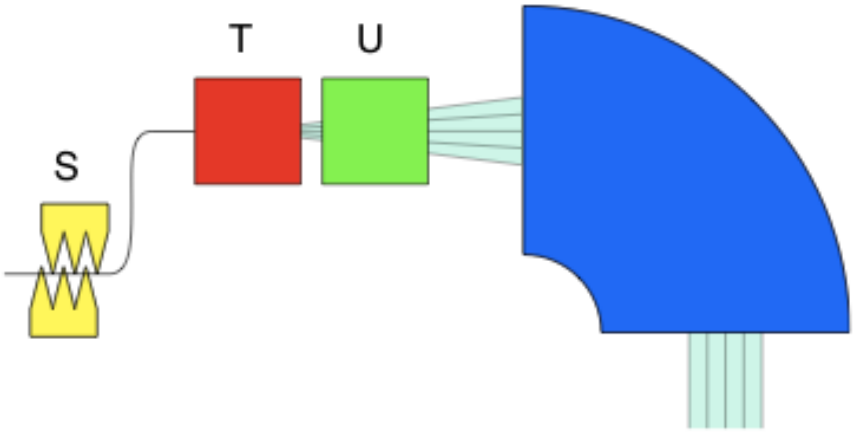

Figure 5: Gantry 2 active scanning representation. On Gantry 2 scanning is performed based on two sweeper magnets (U and T) and an energy degrader system (S). The degrader is situated just after the cyclotron and not on the gantry itself. To change the horizontal direction of the beam to a vertical direction, a 90º bending magnet is used (adapted from [26]).

All of these techniques are controlled by the specifications implemented on the treatment planning systems (TPS). These specifications are translated afterwards to the equipment in order to perform the treatment according the dosimetric plans created. PSI has created its own TPS, named PSIplan, which is constantly under development. The TPS has currently different versions according either the clinical or research interest and the proton therapy gantry used. Like the majority of proton TPSs worldwide, PSIplan uses analytical algorithms as the core basis for dose calculations. Concerning the clinical data needed for the calculations, PSIplan uses binary files as input. For instance the DICOM planning CT obtained from the CT scanner is converted to a specific file format defined at CPT, which is a binary file with the extension CTCT, full of integers representing the scaled Hounsfield units. The HU start at -1000, however, within CTCT file the scaled HU are used, which are shifted +1000 values (explained in 2.6 sub-chapter).

PSIplan is able to calculate different dose distributions according the clinical specifications. These dose distributions may be calculated using the SFUD technique or IMPT. Additionally, it has integrated some optimization tools such as the robustness plan tool (sub-chapter 3.2.1).

2.5. Range uncertainties

One important characteristic in proton therapy that should be pointed out is that the clinical evaluation of the calculated dosimetric plan is always done through the data obtained from a software. In fact, even with the more sophisticated calculation algorithms, this is not only more, at the best, than an approximation of the dose that is in truly delivered to the patient as well as of the position where this dose is deposited. This is a reality not only for proton therapy but also for conventional radiotherapy. Therefore, uncertainties along the treatment process are inevitable [24]. Some of these uncertainties such as the patient position, are random in nature and are thus mitigated along the fractionated treatment, however, systematic uncertainties are part of the treatment process and can be potentially more critical.

As introduced, the exploitation of the proton beam steep fall-off and consequent finite range is the main advantage of proton therapy, allowing great conformal dose distributions. Nevertheless, the location of the Bragg-peak is not always well predicted, specially for complex patient geometry, and small variations in the proton beam range can potentially cause substantial over-dosage of the healthy tissue or an under-dosage of the target volume (the dose delivered should be within 5% of the dose prescribed). The causes of this uncertainty have been therefore highly investigated in order to be minimized since a reliability on an accurate determined depth is fundamental [3, 24]. Range uncertainties arise from four different sources: organ motion, setup and anatomical variations, dose calculation approximations and biological considerations [4].

Firstly, there are uncertainties in the range, random in nature and independent of the dose calculations. Specifically, they are caused by variations of the patient position and beam reproducibility. The latter one has generally a small magnitude (influence of ±0.2 mm in the range), but the patient setup has already a relevant influence of ±0.7 mm in the range, which can be increased in the presence of high heterogeneities [4]. Again, due to their random nature they tend to blur out under the typical fractionated treatments. The commissioning process also introduces an uncertainty (±0.3 mm), which is systematic, and patient anatomy changes, despite being generally random, can be systematic (for instance tumor shrinkage) and have gradual but severe effects in the range during the treatment process [2, 4].

Still independent of the dose calculations are the range uncertainties caused by biological effects. Specifically uncertainties due to variations in RBE. The RBE value is not constant, depends on several physical and biological properties, but in proton therapy it is used an average invariable value,

as referred in the 2.1.2 sub-chapter. This approximation is responsible for an uncertainty in the range of around 0.8% [3, 4].

There are also range uncertainties due to MCS algorithm limitations. The extent of these uncertainties are dependent on the TPS calculation method, i.e., whether it is based on Monte Carlo simulations or in analytical algorithms. At PSI, as well as in most proton therapy facilities, analytical algorithms are implemented within the TPS mainly because they are extremely fast compared with the actual Monte Carlo TPS systems. Concerning analytical algorithms, they generally project the range based on water equivalent depth and are less sensitive to abrupt density variations such as bone-tissue interfaces. The range degradation effect is then not well modeled by these algorithms resulting in a range uncertainty of around 1.5 mm (-0.7%). In fact these effects can be much more negative. In complex structures with high heterogeneities, such as the skull, the range can be reduced by up to 8 mm [4].

Finally, the treatment planning systems (TPS), as in conventional radiotherapy, use CT images as a basis for treatment planning. Range calculations are then dependent on the limitations of CT image acquisitions such as image noise or reconstruction artifacts. This uncertainty is around ±0.5% of the range for modern CT scanners [4]. Additionally, in proton therapy the CT Hounsfield units must be converted to relative proton stopping power values (sub-chapter 2.5). Even though sophisticated methods and algorithms have been developed to do this conversion, there are still relevant approximations that add a considerable uncertainty in the calculation of the range [2]. First, the uncertainty in the range due to the stoichiometric conversion itself (the one used for the CT calibration at PSI) was estimated as ~0.5%. Second and more important, there are a relevant uncertainty in the calculation of the stopping power values due to variations of the mean excitation energy (I-value). These variations are responsible for an uncertainty in the range calculation of ~1.5% for tissues [4]. Taking into account all of these CT parameters, the range uncertainties caused by a well calibrated good quality CT are in the order of ±3% [2].

2.6. CT HU to relative stopping power

Treatment planning systems, which take into account the tissue inhomogeneities, require information about the anatomical structures in order to be able to calculate dosimetric plans. Since the advent of proton therapy, this anatomical data has came indirectly from CT imaging. CT imaging provides a 3D spatial map of voxels representing the patient's anatomy together with a CT number expressed in Hounsfield unit (HU). The HUs represent the relative tissue attenuation of x-rays in water and is given by [27]:

$$HU = \frac{\mu - \mu_{H_2O}}{\mu_{H_2O}} \times 1000 = \frac{1000\mu}{\mu_{H_2O}} - 1000 \qquad (2.5)$$

They start at -1000 (the HU value for air). The value 0 is the HU of water and higher values correspond to materials with photon attenuations greater than the attenuation for water.

The properties of the physical interaction of protons with matter define the analytical algorithms and the physical parameters required for the calculations within the TPS. Concerning proton therapy, the simulation of the interaction of protons with the matter, necessary for the TPS calculations, uses the relative stopping power values of tissues to water, which must be converted from the HU of the CT image.

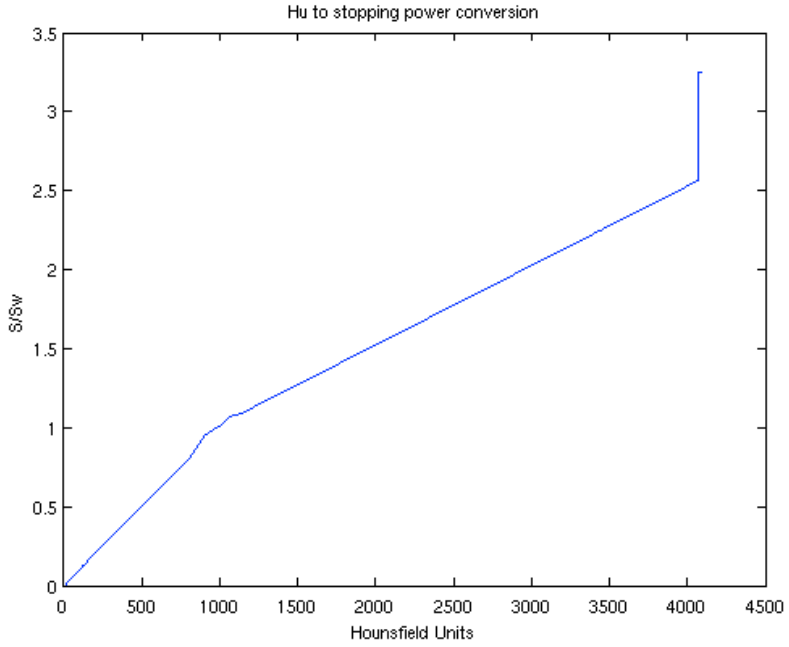

Figure 6: Calibration curve used at PSI obtained under the stoichiometric method [28]. Here are used the scaled HU. The graphic was obtained through the manipulation of the CBSP binary file integrated within TPS, which represents the relative stopping power values to water.

At PSI this conversion is made through a calibration curve determined at time of CT commissioning, which was obtained under the stoichiometric calibration method proposed by U. Schneider et al [28] and is implemented in PSI treatment planning system (PSIplan) (figure 6). This calibration curve relates the scaled HU values to a specific relative stopping power value. The scaled HU are shifted +1000 HU values, being thus the HU value of air converted to 0 whilst the HU of water to 1000. In this conversion curve the scaled HU higher than 4000 are converted to the relative stopping power of titanium (figure 6).

3. Materials and Methods

In this chapter it is discussed the procedures created to accomplish the goal proposed and all the materials used during the project, specially the description of the detectors. To preform clinical treatments as well as experimental measurements with a proton therapy gantry, an extensive planification and dosimetric planning is required.

The project can be divided into two sections: the experimental procedure and the analysis procedure (figure 7). The first one corresponds to the CT HU changes, the dosimetric planification of the different scenarios, plan submission and finally the correspondent experimental measurements with the different detectors. The analysis procedure is the creation of new dosimetric plans along with its submission to the PSIplan robustness tool in order to analyze and compare them with all the measurements scenarios.

3.1. Experimental procedure

In order to be able to measure dose on the surface of a phantom “skin”, one can simple create a dosimetric plan, use it as input for the gantry and place the dosimeters on the desired place. This procedure however, might not be enough to actually allow the dosimeter detection of a significant amount of dose that can be used to compare with the dose predicted by the TPS. Due to this reason the overshooting scenarios were created. Additionally, they also lead the evaluation of the effect caused by +3% range-error, simulating the uncertainty value used at PSI.

3.1.1. Overshooting scenarios development

To experimentally evaluate the effect of range uncertainties in a dose distribution, using the EIVD method, they must be deliberately created in order to create an experimental overshooting

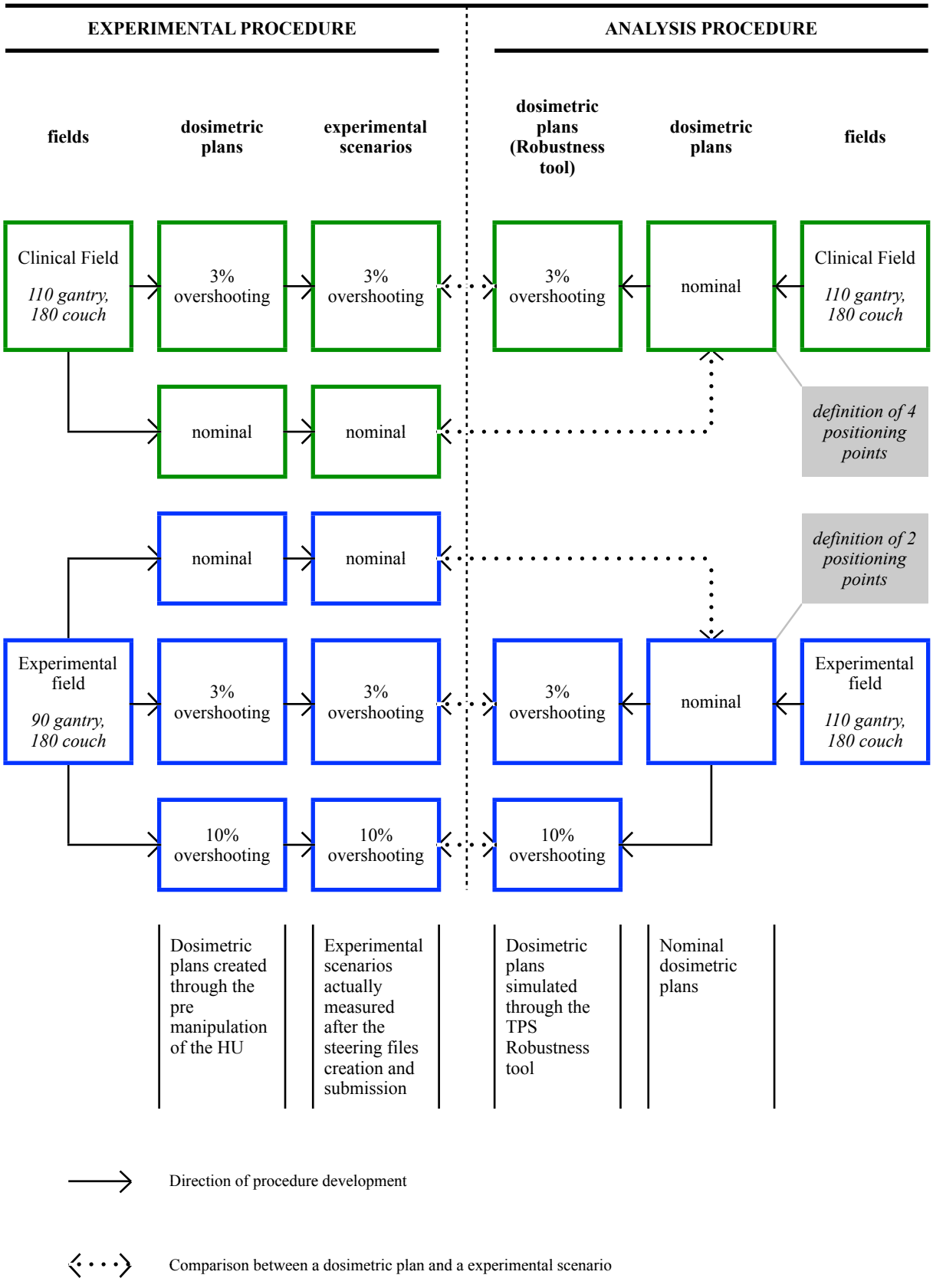

Figure 7: Diagram summarizing the work method procedure. The green boxes correspond to the method 1 while the blue boxes to the method 2.

scenario. To perform that, the proton range should be indirectly controlled and increased. Actually, several methods could be applied simply because there are multiple sources of range uncertainties, however, as referred in the chapter 2.5, CT HU conversion to relative stopping power is one of the main causes of uncertainties. Therefore, it was chosen to be used as the simulation tool to indirectly increase the range.

At CPT this conversion is done through the stoichiometric calibration curve which is inserted within TPS by a binary file [28]. The values within the CT binary file (CTCT file), representing theHU of the planning CT, are the data necessary to calculate the relative stopping power, which in turn are the input data for the dose calculation algorithms. Changing the CTCT file HU values changes, perforce, the relative stopping power used for each tissue. Specifically, changing the HU of a CT for instance by +3% will cause the increase of the relative stopping power according the calibration curve implemented within TPS (figure 8). This changes were then performed in the nominal CT and these modified CTs were used for TPS dosimetric calculations in order to create the dosimetric plan required to experimentally simulate an effect of the range uncertainties, an overshooting scenario.

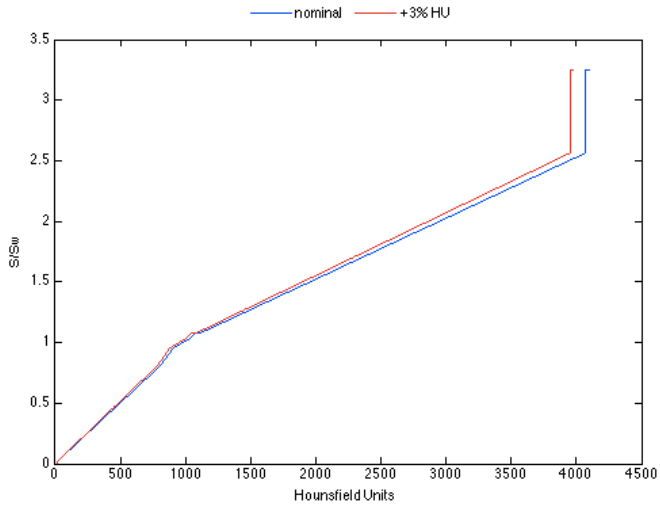

Figure 8: Calibration curve used at PSI obtained under the stoichiometric method (blue) [28]. The red calibration curve corresponds to the values of the relative stopping power due to a change of +3% in each HU value.

As a matter of clarification, despite the algorithms characteristics implemented, this overshooting scenario is actually predicted and easily explained. Physically, to achieve the same beam range in two materials with different stopping power values it is necessary for the material with higher values of stopping power, higher values of beam energy, maintaining the remaining beam characteristics unchanged. Therefore, in dosimetric plan calculations, when all the stopping power values calculated from the CT image are respectively higher than the nominal values, which is the case, the resultant field energy increase in order to cover the target according the same prescription and constrains. At the time of experimental measurements, this modified beam interacts with the phantom, which as the nominal stopping power values, causing the desired overshooting scenario.

In the context of the project the changes were set to be 3% and 10% of the CTCT nominal HU values. These changes imply a considerable change in the relative stopping power values and consequently in the experimental dose distribution of the fields, which will be out of the phantom, and significantly measurable by the dosimeters.

3.1.2. Dosimetric plans

In order to perform the required measurements several dosimetric plans were created using PSIplan for Gantry 2. The dosimetric plans were made using a CT image taken from a head phantom. Three CTCT files were used each one with different HU values:

- "Nominal scenario": The nominal CT image, corresponding to the default CTCT file of the phantom.

- "3% overshooting scenario": A CT image with +3% of each nominal CT image value. The nominal CTCT file was read with Matlab®, modified and then rewritten. The 3% corresponds to the error margin adopted for proton range.

"10% overshooting scenario": A CT image with +10% of each nominal CT image value. As well as for the latter CT image, the nominal CTCT file was read using Matlab®, modified and then rewritten. The reason for a scenario with this order of percentage is explained on the sub-chapter 3.1.4

On the planning CT two targets, corresponding to the tumor area and two regions representing the organs at risk, were simulated. These same target and OAR configuration was used during the entire set of experiments.

Additionally two different fields were chosen to perform the dosimetric plans according the configuration of the experiments:

- A clinical field with 110 degrees of gantry rotation and 180 degrees of couch rotation.[2]

- A experimental field with 90 degrees of gantry rotation and 180 degrees of couch rotation. The choice of this field is related with the positioning issues of the dosimeters used in the experiment.

The following table sums up the dosimetric plans created for the experimental measurements with the dosimeters:

[2] Other clinical fields not presented in this thesis were created, however, the latter one was evaluated as the best for the purposes of the experimental measurements planned

	Scenarios	Field
1	nominal scenario	110º gantry, 180º couch
2	3% overshooting scenario	
3	nominal scenario	90º gantry, 180º couch
4	3% overshooting scenario	
5	10% overshooting scenario	

Table 1: Summary of the 5 dosimetric plans created with the PSIplan for the experimental measurements

For each one of the dosimetric plans the respective steering files were created and submitted, in order to be able to run the experimental treatment at Gantry 2.

3.1.3. Method 1 - Detector on the surface of the skin

The first measurements were performed with the most direct approach, placing the detectors on the surface of the phantom in different points. For these first measurements it was used both the TLDs and the Semiflex IC. The TLDs have good physical characteristics for the EIVD approach (portability and small size) and the IC was used as reference dosimeter. According with the characteristics of this method and the dosimeters intended to be used, 2 scenarios were evaluated:

- Nominal scenario, planned with the nominal CT;

- 3% overshooting scenario, planned with the CT with +3% of the nominal HU.

As described in the 3.1.2 section, the clinical field (110 degrees of gantry rotation and 180 degrees of couch rotation), which was found to be a suitable field for the measurements, was selected for these set of experiments. The dose prescribed according to the field was 0.5 Gy, corresponding to0.45 Gy(RBE). During the the experimental measurements the dosimeters were placed on 4

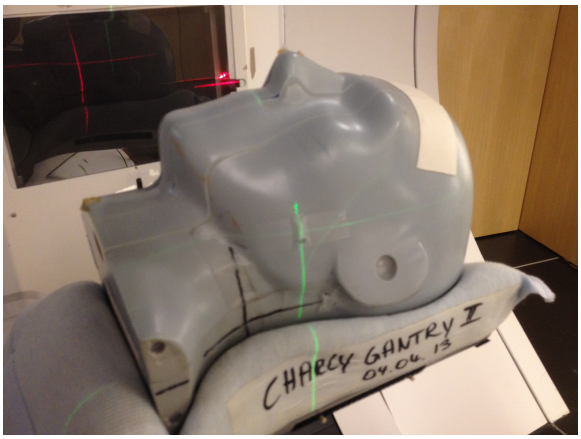

Figure 9: Image of the TLD positioning on the skin of the phantom preformed with the help of the positioning lasers system.

different points that were evaluated during the analysis procedure (sub-chapter 3.2.2). This positioning was made with the support of the positioning lasers system existing in the treatment room (figure 9).

Concerning the IC, the measurements were performed 3 times and then averaged. TLDs measurements however, were not reproduced since TLDs can not be used again after an irradiation. They must be first subjected to a extensive readout process and then erased in order to be used again.

3.1.4. Method 2 - 2D array approach

A second method using the 2D array detector as reference was planed in order to overcome essentially the position errors inherent to the detector positioning method, which become more evident after the evaluation of the method 1 results. The 2D array has the ability to measure the dose in a plane, therefore it is possible to evaluate the dose not only in a specific point but also in the 729 ICs, leading to the possibility of creating a 2D map of dose. Additionally to the 2D array, 4 other detectors were also used: 2 ICs (Semiflex and Advanced Markus), the diamond detector and the TLD.

For this method three different scenarios were created:

- Nominal scenario, planned with the nominal CT;

- 3% overshooting scenario, planned with the CT with +3% of the nominal HU;

- 10% overshooting scenario, planned with the CT with +10% of the nominal HU.

As described in 2.3.4, the window thickness of the 2D array, 9.3 mm of WET, should be taken into account. Since the measurements were made in the distal fall-off region of the Bragg-peak, this entrance window, made of PMMA, is thick enough to do a significative modification on the beam, stopping a high percentage of protons so that the ICs under it would not detect any dose. Thereby, in order to make sure the range would be increased and it would be possible to detect a significative amount of dose, the 10% overshooting scenario was created.

Due to the position limitation of the 2D array, instead of the clinical field, a experimental field (90 degrees of gantry rotation and 180 degrees of couch rotation) was used. The dose prescribed to the target as influence of the field was 1 Gy or 0.91 Gy(RBE). The 2D array was set up perpendicular to the beam, over its own lateral face, and the point dosimeters were placed over it surface when the measurements took place (figure 10).

Unlike method 1, where the points were chosen analyzing the plans created in the analysis procedure, the detectors were placed in two different places (figure 11) chosen through the analysis of the 2D array measurements results:

- Point E: Over the central IC of the 2D array (array coordinates: row (R)=14, column (C)=14);

- Point F: Over the 2D array IC where it was found out to be the point with the highest dose (array coordinates: R=12,C=11).

In this method all the measurements were reproduced 3 times for all the dosimeters, except for the TLD, due to the same reason explained in the sub-chapter 3.1.3.

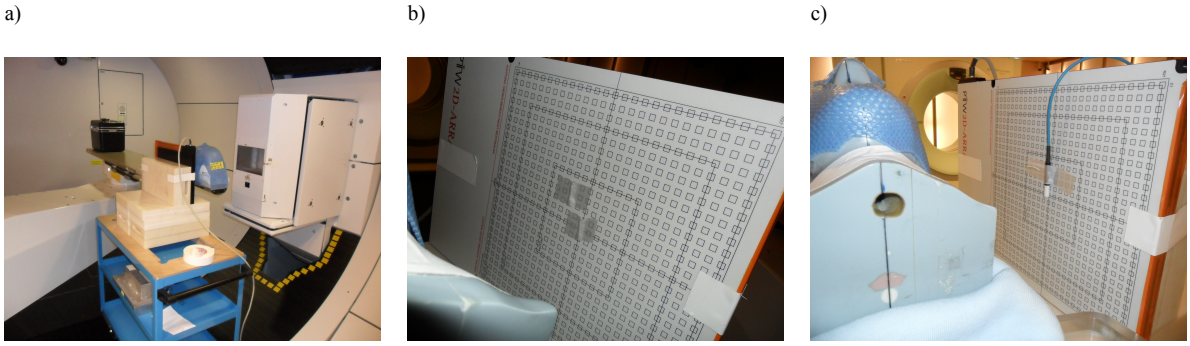

Figure 10: a) Image of the general set up of the experiments. The 2D array was placed behind the gantry point of view. b) procedure concerning the placement of the TLDs. They were placed over the 2D array in the 2 points of dose evaluation. c) representation of the diamond detector positioning method in the central point (R=14, C=14). The ICs were positioned using the same method.

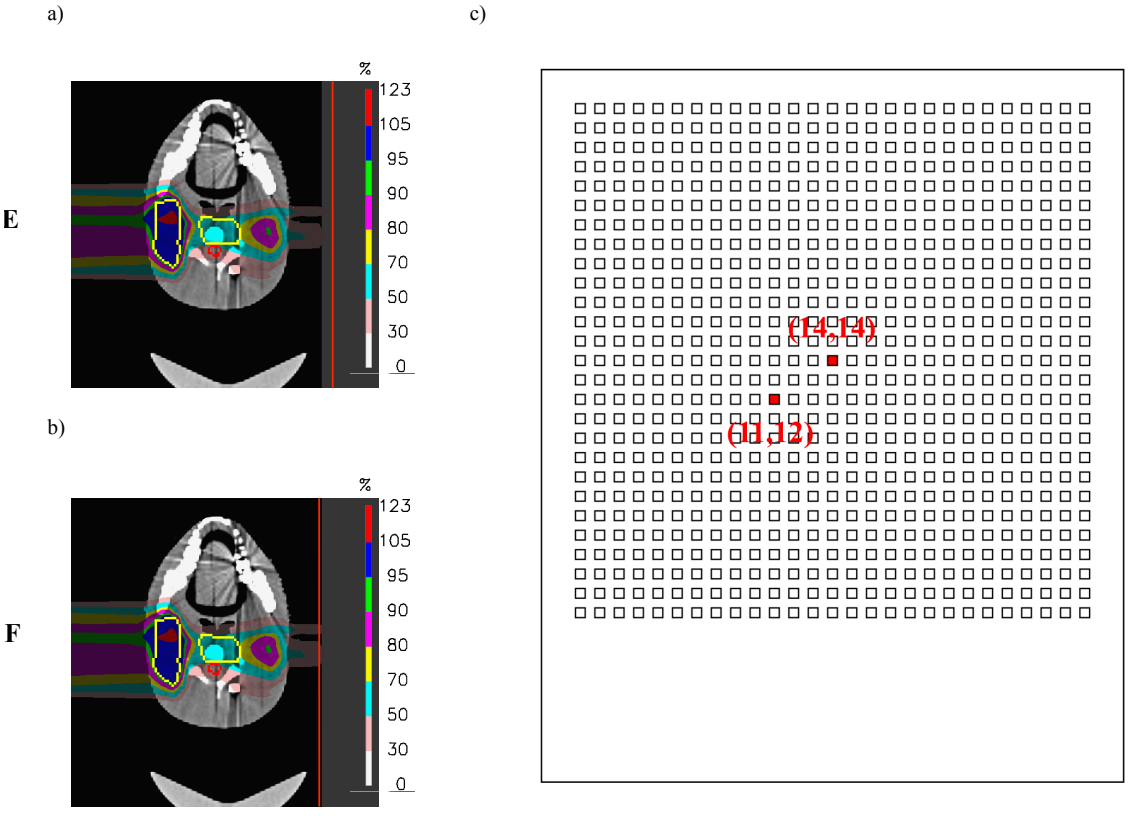

Figure 11: Representation of the detector position in the nominal scenario. a) for the 2D array the dose in the TPS was evaluated 9.3 mm WET inside the entrance window (grey). The CT coordinate in x direction is X=171. b) For the point dosimeters, in the TPS, the dose was evaluated on the surface of the entrance window (grey). The CT coordinate in the x direction is X=166. c) graphical representation of the 2D array. The red squares correspond to the position of the 2 points were the dose was evaluated.

3.1.5. Dosimeters

Several dosimeters with different characteristics were tested in the project. Four point dosimeters: thermoluminescent dosimeters (TLD), a diamond detector, a standard ionization chamber (IC) and a plane parallel ICs. Additionally, the feasibility of a 2D array detector was also tested.

3.1.5.1. Thermoluminescent dosimeter (TLD)

Thermoluminescent dosimeters are commercial available in various forms (e.g. powder, rods, chips and ribbons) and are made of different materials.TLDs operate based on the properties of some materials which, upon absorption of radiation retain part of that energy in metastable states. Specifically, TLDs have a storage trap structure, made of impurities and imperfections, that depends on the crystal used (most common being LiF:Mg), placed between the valence and conduction band. When the crystal is exposed to ionizing radiation the electrons are promoted to the conduction band,leaving a free hole in the valence band. Then, they migrate along the crystal until they lose energy and become trapped in electron traps [29]. Later on, when reading the TLD, following the excitation by heat, the energy stored in the traps is released in form of light, which can be read by a photomultiplier tube. The amount of luminescence is thus proportional to the absorbed dose received from the ionizing radiation[6].

For the experimental measurements TLD-100 (LiF:Mg,Ti) rod models (Harshaw Chemical Company, Solon, OH) with 1 mm in diameter and 6 mm in length (Figure 12) were used. The readout of the dosimeters were carried out using a TLD annealing oven (PTW, Freiburg, Germany) and a TLD reader (Teledyne Brown Engineering).

Figure 12: TLD-100 used in the experimental measurements.

3.1.5.2. Ionization Chambers

ICs can be found in different sizes and shapes depending on the purpose. The most widely used are cylindrical ICs (thimble IC) and plane parallel ICs, both used in the project. The first ones consist of a gas filled cylindrical cavity surrounded by a conductive outer wall with a collecting electrode in the central axis. The ionizing radiation interacts with the gas creating ion pairs which are then

collected, creating a current that can be read by an electrometer. Parallel plane ICs consist of two conductive walls disposed parallel to each other. The entrance wall is the polarizing electrode while the back wall is the collecting electrode, which is a thin conducting layer of graphite disposed on a non-conducting material [29, 30].

Within the cylindrical IC category it was chosen the PTW Semiflex with a sensitive volume of 0.125 cm^3. It has a diameter of 5.5 mm and 6.5 mm length (figure 13a). The plane parallel IC used was the Advanced Markus, from PTW as well, with a sensitive volume of 0.02 cm^3, a diameter of 5 mm and thickness of 1 mm (figure 13b). Both ICs have an entrance windows of 1 mm and 1.06 mm water equivalent thickness (WET), respectively, calculated in photon beams (figure 13c and 13d) [30].

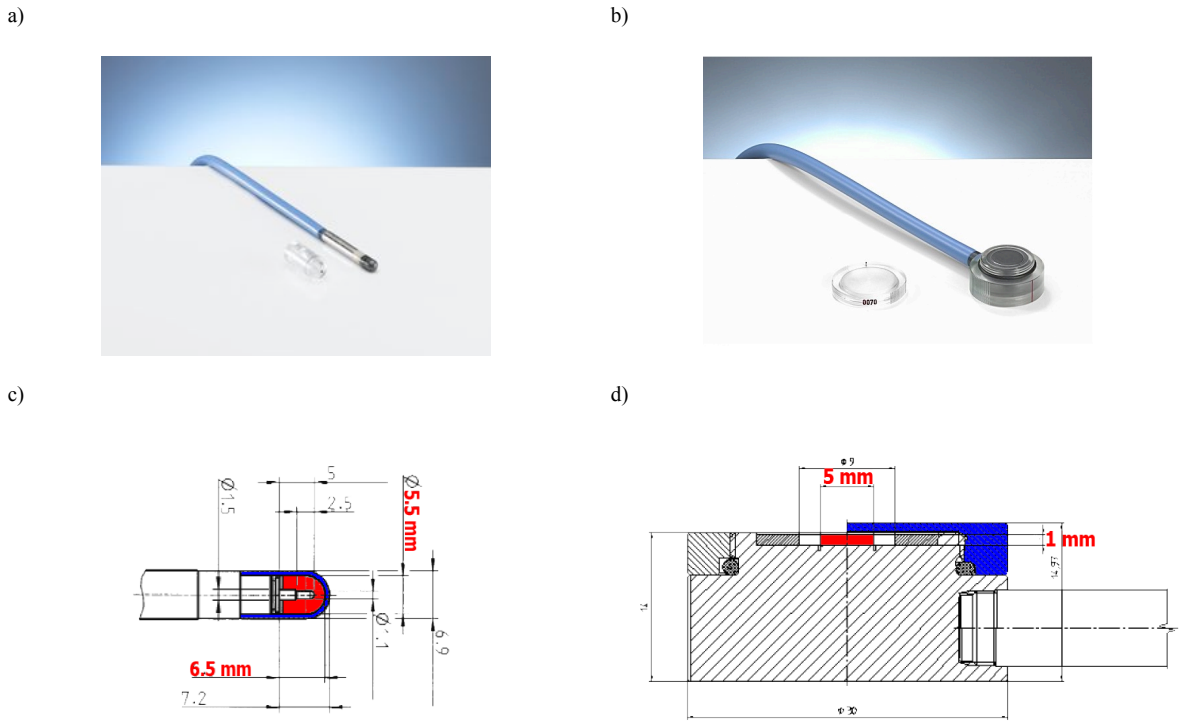

Figure 13: a) PTW Semiflex IC and it schematic representation. b) PTW Advanced Markus IC and the respective schematic representation. In both schematic representations, c) and d), the red area corresponds to the sensitive volume while the blue are to the capsule. The water equivalent thickness of both capsules is around 1 mm (adapted from **[30]**).

3.1.5.3. Synthetic Single Crystal Diamond Detector (SCDD)

Diamond detectors hold a synthetic single crystal diamond structure which is a material ideal to build small volume high-resolution solid state detectors. Due to the diamond properties such as tissue equivalence, requirement of almost no energy correction, very good energy response and negligible directional dependence, they have been considered promising for relative dosimeter with proton beams and can be used in high dose gradient regions [29, 31].

The SCDD used in the project was a test version from PTW built in collaboration with the Tor Vergara University in Rome (figure 14a). The detector structure consists basically of a deposition of three layers of a synthetic single crystal diamond, with different characteristics, followed by a aluminum layer in order to form a diode. This detector operates with no external bias voltage since there is a built-in potential at the diamond interface with the metal [31]. Specifically, when the incident radiation interacts with the diamond, positive and negative charge carriers are sorted out by the field of the diode. These charges produce a current which can be measured afterwards by an electrometer [32].

The diamond volume is 3 × 3 × 0.3 mm^3 but the sensitive volume corresponds to the junction region extended through the thickness of the upper diamond layer below the whole circular metal contact (figure 14b). This sensitive volume is 0.004 mm^3. The housing of the detector is made of polymethyl methacrylate (PMMA) with 7 mm diameter and 45.5 mm length. The WET of the entrance window is 1.1 mm calculated in photon beams [31, 32].

a) b)

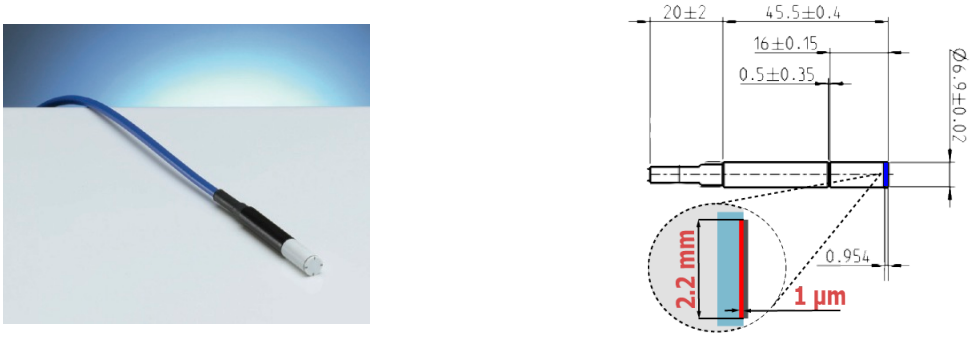

Figure 14: a) SCDD test unit of PTW. b) Schematic representations with the size of each part of the diamond detector. The red area (zoomed in) corresponds to the sensitive volume while the blue are to the capsule. The WET of the capsule is around 1.1 mm (adapted from **[30, 32]**).

3.1.5.4. 2D detector array

The 2D detector array is a two dimensional device with 729 ICs arranged in a 27 by 27 matrix (figure 15a). They have cubic shape with 5 × 5 × 5 mm3 and are equally spaced by 1 cm centre to centre, covering a area of 27 × 27 cm2 (figure 15b). The sensitive volume of each IC is 125 mm3. The surrounding material is PMMA and the window thickness of the 2D array is 5 mm, being the reference point of each IC located at the same distance below the surface. This window thickness for the detector used in the experiences was measured in-house, in order to find the value in proton beams, and corresponds to 9.3 mm of WET [33].

a) b) c)

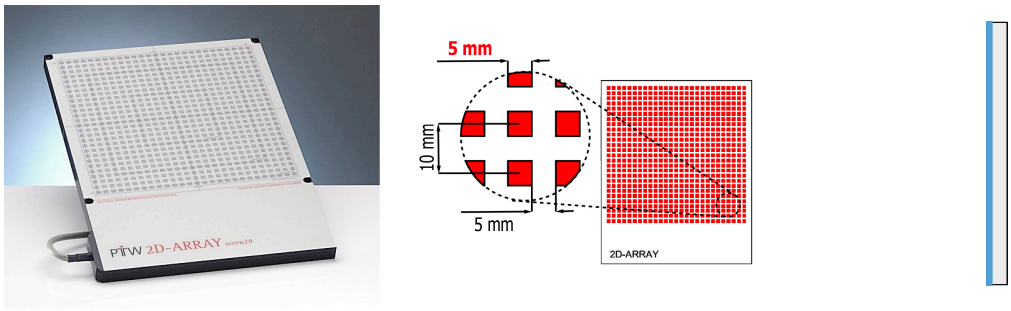

Figure 15: a) PTW 2D array detector (adapted from **[30]**). b) Schematic representation of the ICs, their size and the distance between them. The red color represents the sensitive volume of the PTW array. c) Representation of a lateral schematic view of the PTW 2D array detector. The blue area represents the window thickness with a 9.3 mm WET.

The 2D array detector was used mainly because of its ability to create planar dose measurements of the proton beams (2D maps). This feature is able to overcome positioning errors inherent to the point dosimeters placement method. On the other hand, the placement of the 2D array is not as flexible as it is for the point dosimeters, thus implying a set up of a specific experimental dosimetric plan (sub-chapter 3.1.2 and 3.1.4). Another design drawback of this detector is it relevant window thickness. This window thickness, corresponding to 9.3 mm of WET, should be taken into account when analyzing the dose projected by the TPS (figure 15c). This thickness is big enough to cause an energy loss while the beam crosses it, making considerable dose changes between the dose at the IC depth and the dose at the surface of the array. Consequently, the simulation of this window thickness must be done.

3.1.5.5. Characterization of non-standard dosimeters

Within the 5 different detectors used for the experimental measurements, the ICs (including the 2D array) are the only dosimeters standardized by the International Atomic Energy Agency for proton beams [34]. For that reason they can be used as reference dosimeters. Therefore, TLDs and the diamond detector should be characterized relatively to the IC.

TLDs dosimeters, each one with a calibration factor, were characterized, measuring a dose profile in depth and comparing it with IC. To measure the dose in depth, 20 TLDs were placed in a spiral shape inside a PMMA (density: 1.18g/cm3) cylinder and spaced in depth. The cylinder was then fitted in a PMMA cube phantom adapted for such purpose. The same measurements were done with the PTW Advanced Markus IC placed in a specific mechanism specially made to measure dose in depth. The measurements were performed in the horizontal beam in OPTIS 2 and two different depth dose approaches were set up: a single Bragg peak measurement, without modulation wheel and a dose of 1 Gy to a calibration depth of 16.65 mm; and a SOBP, with modulation wheel and a dose of 1 Gy to

a calibration depth of 22.80 mm. The energy of the beam was 64.26 MeV, calculated using the range of the beam measured with the IC software interface.

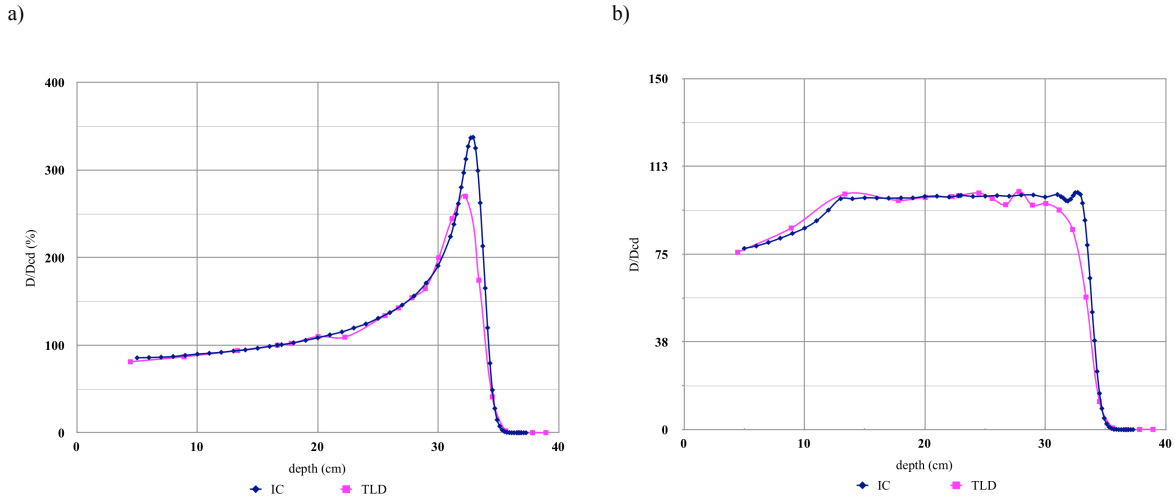

Figure 16: a) Comparison of a single Bragg peak depth dose curve between TLDs and IC measurements. Normalization at the calibration depth of 16.65 mm. b) Comparison of a depth dose curve of a modulated proton beam (SOBP) between TLDs and IC measurements. Normalized at the calibration depth of 22.80 mm.

The results of TLDs characterization are presented in the following graphics (figure 16a and 16b), which compares the single Bragg peak and SOBP depth dose curve of the TLDs with IC measurements. The data are normalized at the correspondent calibration depth - 16.65 mm for the single Bragg peak and 22.80 mm for the SOBP.

The results show an agreement between both dosimeters on the first half of the path. For the first measurements, the Bragg peak depths determined from IC and TLDs were 33.45 mm and 32.89 mm, respectively. So, the difference between both measurements is within 2%. Regarding the SOBP measurements the range calculated agreed within 3% (the depth of the IC measurements is 33.29 mm and the TLDs measurements is 32.15 mm). It is clear in both graphics the under-response of TLDs in the peak and fall-off zone. TLDs and other dosimeters usually show this Bragg peak quenching resulting from an energy-dependent response [3].

The procedure for the characterization of the diamond detector was different than the one used for the TLDs. The characterization was made in Gantry 2 using a water scanning system which allows to measure dose in depth. Two experimental measurements were performed using a 70 MeV beam, the first with the PTW Semiflex IC attached to the water scanning system and the second using the diamond detector. Depth dose measurements were calculated for both dosimeters in order to compare the results of the diamond detector with the reference IC results and find a calibration factor for the diamond detector. The calibration factor calculated was 1.4795E+09 Gy/C. The results are graphically represented in the figure 17. They show a very good agreement between the response of the diamond

detector when compared with the IC. The difference in the measured range is around a tenth of millimeter.

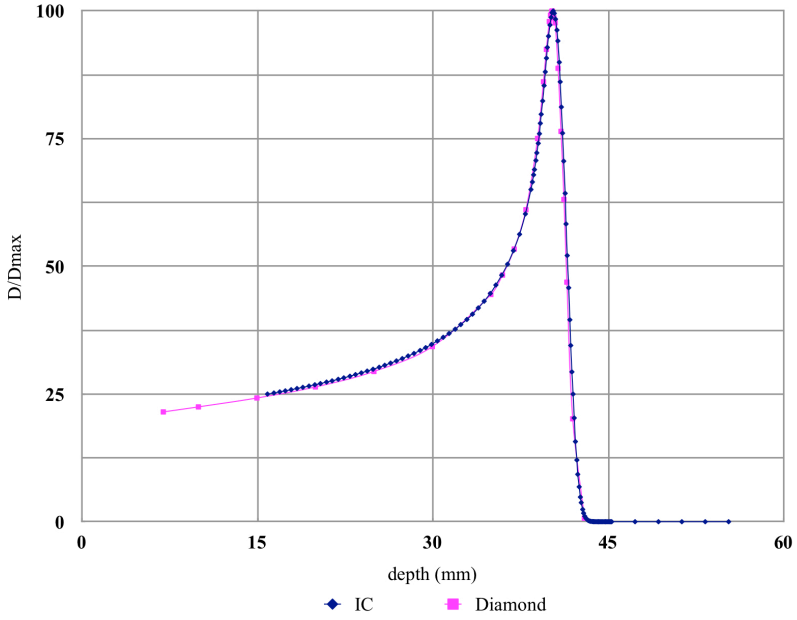

Figure 17: Depth dose curve measured with a water scanning system using the reference IC and the diamond detector. The results show a good agreement between both detectors.

3.1.5.6. Dosimeters global evaluation

The dosimeters referred in this chapter show different advantages and disadvantages for the EIVD approach. Despite that, all of them were used in order to find which one could be better applied in the approach. The following table summarizes a relative qualitative evaluation:

	Advantages	Disadvantages
TLD	Portability; Easy to place on the patient. No voltage is applied	Under-response on the Bragg peak fall -off region; Post-processing is necessary; High probability of positions errors due to the encapsulation and the size of the dosimeter.
IC (Semiflex and Markus	Good reproducibility; Good dose linearity; On-line results.	Unpratical placement; Probability of position errors; Safety issues due to voltage; Cables are needed.
Diamond detector	Good reproducibility (±0.5%) [31]; Good dose linearity [31]; On-line results; Can be in contact with the patient because no voltage is applied.	Unpratical placement; Probability of position errors; Cables are needed.
2D array	Good reproducibility (±0.5%) [33]; Good dose linearity [33]; On-line results; 2D information.	Unpratical placement; Simulation of the window thickness is necessary; Cables are needed.

Table 2: Relative qualitative evaluation of the detectors used in the experimental measurements. The evaluation was made according the characterization of the dosimeters, throughout the correspondent bibliography and analysis of the experimental method during the experiments.

3.2. Analysis procedure

3.2.1. Robustness plan tool

The robustness plan tool is a software implemented within PSIplan with the goal of improving the robustness of the dosimetric plans. Specifically, this tool allows the re-calculation of the fields characteristics (Bragg-peak selection and optimization) assuming a general error of a certain percentage in the nominal HU values (in the project a percentage of +3% and +10%). Then, these optimized re-calculated fields are used to calculate the final dosimetric plan in the nominal CT in order to simulate the effect of the range uncertainties [3, 35].

In the context of the project this tool can be used to simulate the overshooting scenarios created for the experimental measurements, simulating a dosimetric plan where can be analyzed the effect of a

modification of 3% or 10% in the HU. Therefore, and as a matter of clarification, these simulated overshooting plans are indeed different from the ones created in the experimental procedure. Actually, these simulated overshooting dosimetric plans obtained from the robustness plan tool adopt the same field characteristics of the experimental overshooting plans in order to calculate a dosimetric plan in the nominal CT, which will naturally lead to a overshooting simulated scenario. It is in fact a simulation of what happens in the real experiments.

3.2.2. Method 1 - Detector on the surface of the skin

To analyze the dose distributions a nominal evaluation plan was created under PSIplan, with both the clinical field and the dose prescribed referred. The correspondent overshooting plan (3% overshooting plan) obtained from the robustness plan tool was calculated, in order to not only be used to evaluate the dose predicted by the TPS but also to define the 4 points where the dosimeters were placed for measurement (sub-chapter 3.1.3). These points were located in a region where could be feasible to accomplish the goal established (figure 18). Consequently, the following points were selected:

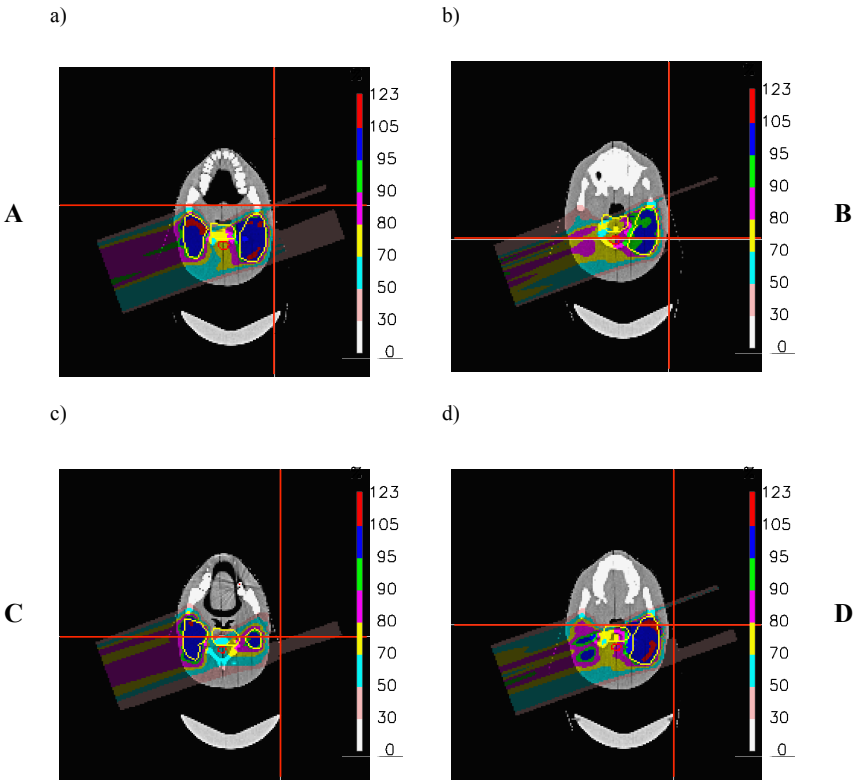

Figure 18: Representation of the detector positions in the nominal scenario and dose distribution obtained using the robustness plan. a) Point A; 1st point in the direction of the field. CT coordinates: 158, 148, 111. b) Point B; 2nd point in the direction of the field. CT coordinates: 159, 121, 104. c) Point C; point with the greatest dose difference between the nominal and the overshooting plan. CT coordinates: 162, 130, 117. d) Point D; point with almost no dose in the nominal plan. CT coordinates: 162, 137, 107.

- Points A and B: 2 points in the direction of the field;

- Point C: point with the greatest dose difference between the nominal and the 3% overshooting plan obtained from the robustness plan tool;

- Point D: point with almost no dose in the nominal plan.

Finally, so that the goal could be accomplished, all the experimental measured results were directly compared against the results from the nominal and overshooting plans obtained in the analysis procedure. This comparison was the tool to understand the extent of the uncertainty in the range for each field.

3.2.3. Method 2 - 2D array approach

Similarly to method 1, the comparison of the experimental measurements with the nominal and overshooting plans (3% and 10% overshooting) created with the robustness plan tool was also the way of evaluating the effect of the range uncertainties. However, as referred above, there are a relevant interference of the entrance window in the beam range and consequently in the dose measured. Thus, this entrance window should be taken into account before creating the plans for analysis.

3.2.3.1. Simulation of the 2D array entrance window

As referred before, it is necessary to replicate the real effect of the 2D array entrance window thickness within the calculation of the dose in the analysis procedure. To do that, since there is a direct relation between the stopping power values and the HU, given by the calibration curve, the entrance window WET was simulated within the CT image. This simulation can be simply made by replacing the default air HU values of the original CT image (CTCT file) corresponding to the position of the entrance window with the water HU values obtained through the calibration curve.

As described before, the CTCT binary file is the converted CT image used within PSIplan, with an array of values corresponding to the HU of each voxel. Each CT cube used in PSIplan is a group of voxels formed out of 255 slices in the *x* and *y* direction and 171 slices in the *z* direction (figure 19a). In the *x* and *y* direction the slices are spaced by 1.953 mm whilst in the *z* direction they are spaced by 2 mm. Each voxel is actually a cuboid with the dimensions $1.953 \times 1.953 \times 2$ mm^3. As explained above, the 2D array is placed with the front face perpendicular to the beam direction, which corresponds, in CT coordinates, perpendicular to *x* (figure 19a). Thus, the thickness of the entrance window must be created, changing the air HU (0) of a certain number of slices in the *x* direction of the original CTCT, with the water HU (982) (figure 19). This value, 982HU, corresponds to the HU value that is converted to the relative stopping power of water, which is 1, according the calibration curve.

To perform that it was calculated how many slices with 982 HU it is necessary simulate. simply dividing 9.3 mm, the WET of the entrance window, by 1.953 mm. The result is 4.762. This value show that 4 slices with 982 HU should be created along with one slice with 76.2% of the relative water stopping power value (0.762×1). According to the calibration curve the HU value corresponding to a relative stopping power of 0.762 is 764 HU.

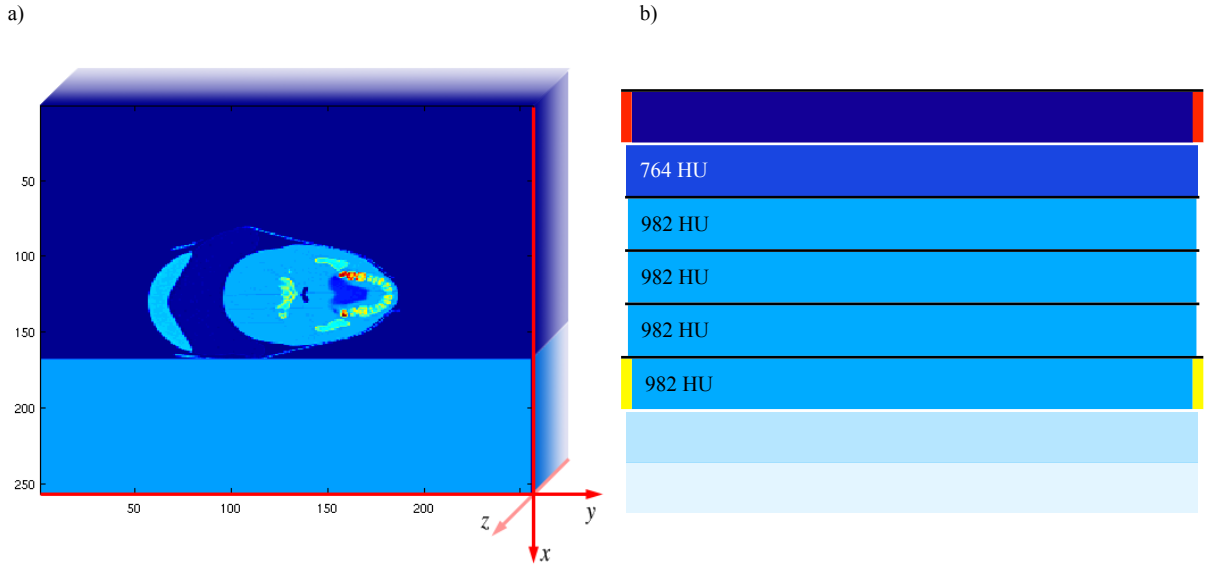

Figure 19: a) Matlab® simulation of the 2D array entrance window. b) representation of the 5 voxel slices of the 2D array. The 764HU voxel slice is represented by the first row (barely visible on figure19a) and the four 982HU voxel slices by the next 4 rows. The red and yellow lines represents the slices were it was measured the dose in the analysis procedure.

Finally this simulation was converted to a CTCT file by a function created in Matlab® in order to be implemented within TPS as a nominal CTCT file. This file was used as input for the robustness plan tool to create the overshooting plans. The dose was further analyzed in two different slices. In order to compare the dose with the dosimeter measurements placed on the surface of the 2D array, the dose was evaluated in the slice representing the 2D array face (slice between the red line in the figure 19b. Slice x=166 figure 19a). On the other hand, to compare with the 2D map obtained directly from the 2D array measurements, the dose was also evaluated behind the 5 voxel slices representing the end of the entrance window (voxels corresponding to the slice between yellow line in the figure 19b. Slice 171 figure 19a).

4. Results

As described in the materials and methods chapter, to find a feasible way to perform the EIVD approach, two methods were implemented. On the first method, the dosimeters were placed directly in the patient and a clinical field was used for the measurements. In the second method it was taken advantage of the 2D array properties in order to perform the measurements. A experimental field was used and dosimeters were placed on the 2D array surface. The idea is to compare the results against the dose predicted by the TPS. In fact, analyzing the potential extent of dose difference between the one planned and the one that is actually measured it is possible to evaluate the feasibility of each dosimeter on the EIVD approach. This chapter gathers the results obtained from the experimental measurements, which were post-processed either through Matlab® or using the respective standard post-processing method.

4.1. Method 1 - Detectors on the surface of the skin

Two types of dosimeters were used in this method: a Semiflex IC and TLDs. They were placed in 4 different points and the measurements were performed using the nominal and the 3% overshooting scenarios. The experimental results were compared with the TPS results obtained through the correspondent analysis plans.

4.1.1. Results

The results are displayed in table 3 and figure 20 show a comparison between the dose predicted by the TPS for 4 superficial points evaluated (red triangle marks in figure 20) against the dose measured by both the IC Semiflex and the TLDs. The IC was not used neither at point B or point D.

A general analysis of the results for all points and scenarios show clearly that the TPS overestimates de dose actually delivered and measured by the detectors. This overestimation, over

	TLD (mGy)	IC (mGy)	TPS (mGy(RBE))	TLD/TPS	IC/TPS	TLD/IC
A						
nominal	95	103	187	0.51	0.55	0.92
overshooting 3%	134	144	235	0.57	0.61	0.93
B						
nominal	23		94	0.24		
overshooting 3%	50		180	0.28		
C						
nominal	18	27	49	0.37	0.55	0.67
overshooting 3%	47	69	159	0.3	0.43	0.68
D						
nominal	0		7	0,00		
overshooting 3%	6		98	0.06		

Table 3: Results of method 1 measurements for the 4 points where the detectors were placed, compared with the ones obtained by the TPS dose distribution. Additionally the ratio between dosimeters and the TPS was calculated as well as the ratio between the two dosimeters.

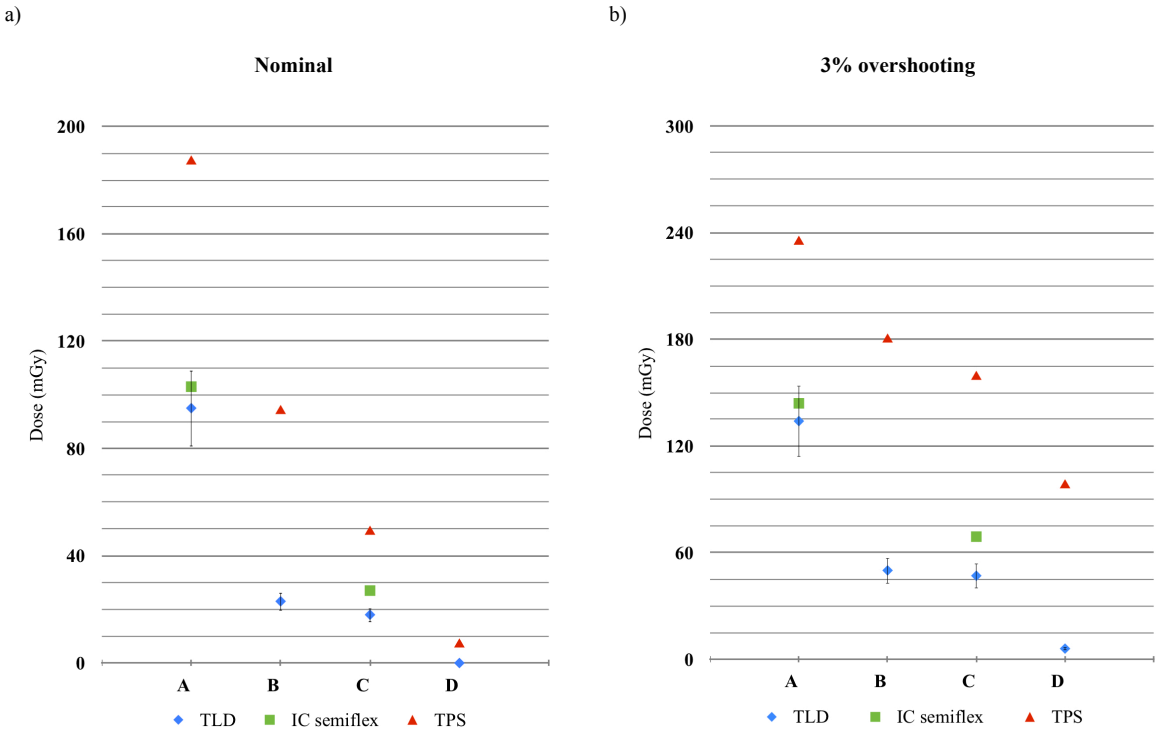

Figure 20: Graphical comparison between TPS prediction results against TLD and IC Semiflex measurements for: a) nominal scenario; b) 3% overshooting scenario. The dose predicted by the TPS takes into account a RBE value of 1.1. The error bar in the TLDs results corresponds to a ±15% accuracy inherent to this TLD model.

twice the value of the measurements - for TLD sometimes around three times its value - is quite significative. Additionally, it is verified that the dose measured by the TLD is always lower than the one detected by the IC Semiflex.

Analyzing in more detail point A from both nominal and 3% overshooting, the dose measured by the dosimeters agree (within the accuracy of the TLD). The ratio is indeed over 0.9 (table 3). However, the dose predicted by the TPS is around twice the real dose (ratio ~0.55 between the detectors and the TPS). Regarding point C, the agreement between the dose measured by both dosimeters do not agree within the 15% of the TLD accuracy but still, the dose predicted is over twice higher than the dose measured (table 3 and figure 20).

4.1.2. Discussion

The results obtained through this method show a considerable difference between the dose predicted and the dose measured, regardless of the detector used.

Concerning the differences between the dosimeters, it is visible the TLDs read always lower dose than the IC. This attribute can be explained by TLDs characterization performed before the measurements, since it was verified the TLDs have an under-response when measuring dose in the high gradient Bragg-peak fall off region (sub-chapter 3.1.5.5).

One of the influences for this big dose variation can be also explained by the dosimeter placement method. In order to position the detectors the lasers existent into the room and integrated within the gantry coordinate system were used, however, it is not possible to precisely place the dosimeters, specially the IC Semiflex, without making some random position error. The effects of this error is still boosted because the measurements are being made in high gradient dose regions, not only in the beam direction due to the fall off region of the Bragg peak, but also laterally to the beam: the heterogeneities of the patient lead often to these lateral high gradients (visible on the dose distributions of figure 16). These latter characteristics of the dose distributions in the exit region of the beam, which in fact belong to the ±3% uncertainty in the range used at PSI, associated with the errors in the positioning of the detectors are actually the main reason for the disparity of dose measured between IC and TLD registered in point C.

4.2. Method 2 - 2D array approach

As explained in the sub-chapter 3.1.4, this method consisted in placing the 2D array perpendicular to the beam in order to measure a 2D map of dose and compare it with the correspondent dose distribution predicted by the TPS. This 2D map, obtained through a specific software and later processed in Matlab®, has a resolution of 27 by 27 pixels, corresponding to the

location of the IC on the array plan. On the other hand the dose distribution from the TPS is a 3D volume with the same resolution and coordinate system as the CT volume (251×251×171 voxels). So, a post-processing of this dose distribution is indispensable so then the experimental results could be compared against the TPS output.

Together with the 2D array measurements four point dosimeters were placed over specific positions: the central IC point (point E: R=14, C=14) and the IC where it was found out to measure the highest dose value (Point F: R=12, C=11). The dosimeters used were two ICs (Semiflex and the advanced Markus from PTW), a diamond detector and TLDs.

4.2.1. 2D array

4.2.1.1. Post-processing of the TPS dose distribution

To manipulate the TPS dose distribution the Matlab® was used. The 3D dose distribution volume, obtained after a dosimetric plan calculation on the robustness plan tool, corresponds to a output file (PTDT extension) with a value of dose in each voxel. As referred in 3.6.2.1, the 2D array dose was analyzed on a PTDT slice corresponding to the same plan where the ICs are placed inside the array, after the 9.3 mm of WET. Practically, according to the CT volume, this slice is the fifth slice in the *x* direction of the simulated 2D array (slice $x = 173$) (figure 21).

For each CT image that is done for treatments, there are a spatial coordinate system associated. In other words, the CT coordinates of the CTCT used to calculate the dose distribution have a respective transformation in room coordinates. Is then possible to relate each voxel with a room coordinate. Taking this into account, the 2D array was positioned with the centre of the central IC (R=14, C=14) in a known room position ($x = 23.20$ cm, $y = -1.11$ cm and $z = -130.6$ cm), which was then translated to the CT referential (x=173, y=121, z=119) in order to directly define which voxel on the dose distribution plan corresponds to the centre of this central IC (figure 21, intersection of the red lines). As described on the sub-chapter 3.1.5.4, the sensitive volume of each 2D array IC is a cube with 5 mm edges. However, each PTDT voxel is a cuboid of 1.953×1.953×2 mm. This means that the volume of a voxel is around 20 times smaller than the IC sensitive volume. Therefore, in order to have a better volume approximation, it was not only taking into account the dose on the referred voxel but also the dose on its adjacent voxels by simple averaging the values.

Afterwards, according to the physical measurements of the 2D array, the location of each IC centre referent to the centre of the central IC was calculated. These coordinate points were then used to find the voxel correspondent to the remaining ICs centers and the same averaging method was performed. Through this pos-processing method it was then possible calculate which predicted dose

volume on the dose distribution corresponds spatially with each 2D array IC. The output of this Matlab® script is a 2D map similar with the one obtained through the 2D array measurements.

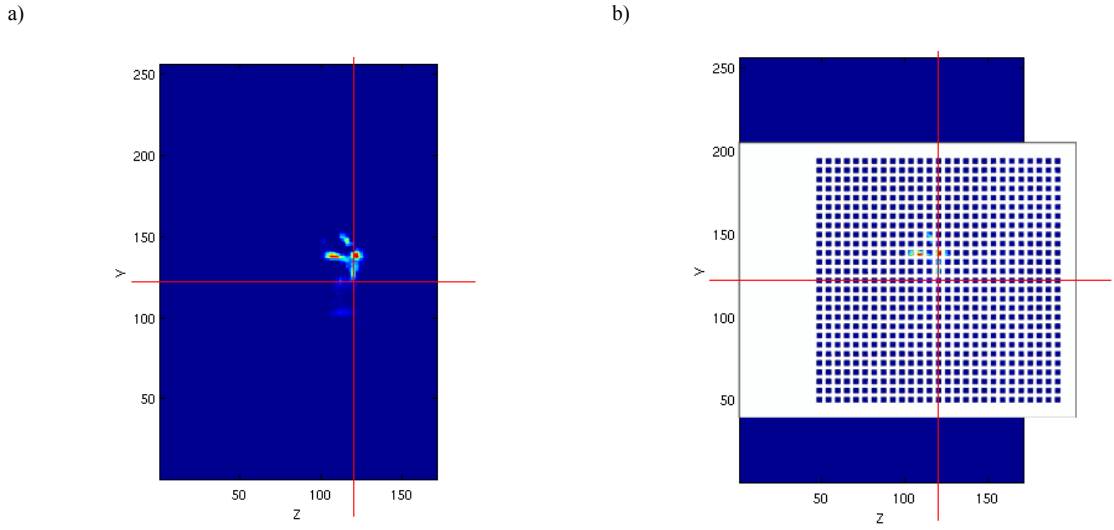

Figure 21: a) Slice *x*=173 obtained from the PTDT file which was created through Matlab® manipulation. The intersection point of the two red lines corresponds to the location of the central IC of the 2D array. CT coordinates: *x*=173, *y*=121, *z*=119. b) Representation of the 2D array over the dose distribution. The voxels on each square (ICs) were averaged in order to have an approximation of the dose measured experimentally.

4.2.1.2. Results

In this approach, along with the nominal and the 3% overshooting scenarios, a 10% overshooting scenario was evaluated. Concerning the 2D array measurements, results are presented as a 2D map of dose standing out the 2 points where the dosimeters were placed, point E and F. The results are presented in the table 4, graphics in figure 22 and set of colormap images (figure 23). In order to better evaluate the results, the dose variation that actually is possible to be verified as a result of the ±3% variation of the range (uncertainty used at PSI) was also added (grey area added to figure 22a).

Analyzing the dose distribution quantitatively the results show a similar behavior with the ones obtained using method 1. Focusing on the point E and F it is verified the TPS predicts much more dose than the one actually delivered (figure 22). Regarding the nominal scenario, the dose measured is not within the dose variation that is possible to be verified (grey area in figure 22a). Analyzing the table 4, the dose predicted is over 5 times higher (ratios lower than 0.2).

Regardless of the scenarios, one can compare geometrically the shape of the 2D maps of the experimental results from the 2D array (left column of the figure 23) with the TPS results in order to evaluate the characteristics of the exit beam. The shape of the dose distribution is considerably different. The experimental dose distribution from the 2D array has a more homogeneous dose

gradient radially to the beam centre, where the highest dose pixels are situated. On the other hand the dose distribution predicted by the TPS shows a slightly different shape, less circular, and more heterogeneous. However, we can assume the centre of the beam is well predicted since the maximum dose was measured on the same coordinate pixels.

	2D array (mGy)	TPS (mGy(RBE))	2D array/ TPS
E (R=14,C=14)			
nominal	6.1 (~0.7%)	29.0 (3.2%)	0.21
overshooting 3%	13.9 (1.5%)	80.8 (8.9%)	0.17
overshooting 10%	44.8 (4.9%)	335.8 (36.9%)	0.13
F (R=12, C=11)			
nominal	27.1 (3.0%)	167.1 (18.4%)	0.16
overshooting 3%	51.2 (5.6%)	306.8 (33.7%)	0.17
overshooting 10%	112.2 (12.3%)	696.6 (76,5%)	0.16

Table 4: Results of the method 2 measurements for the 2D array both for the central IC and for the IC with coordinates (R=12, C=11). The percent values correspond to the percentage of dose measured relative to the dose prescribed, 910 mGy(RBE).

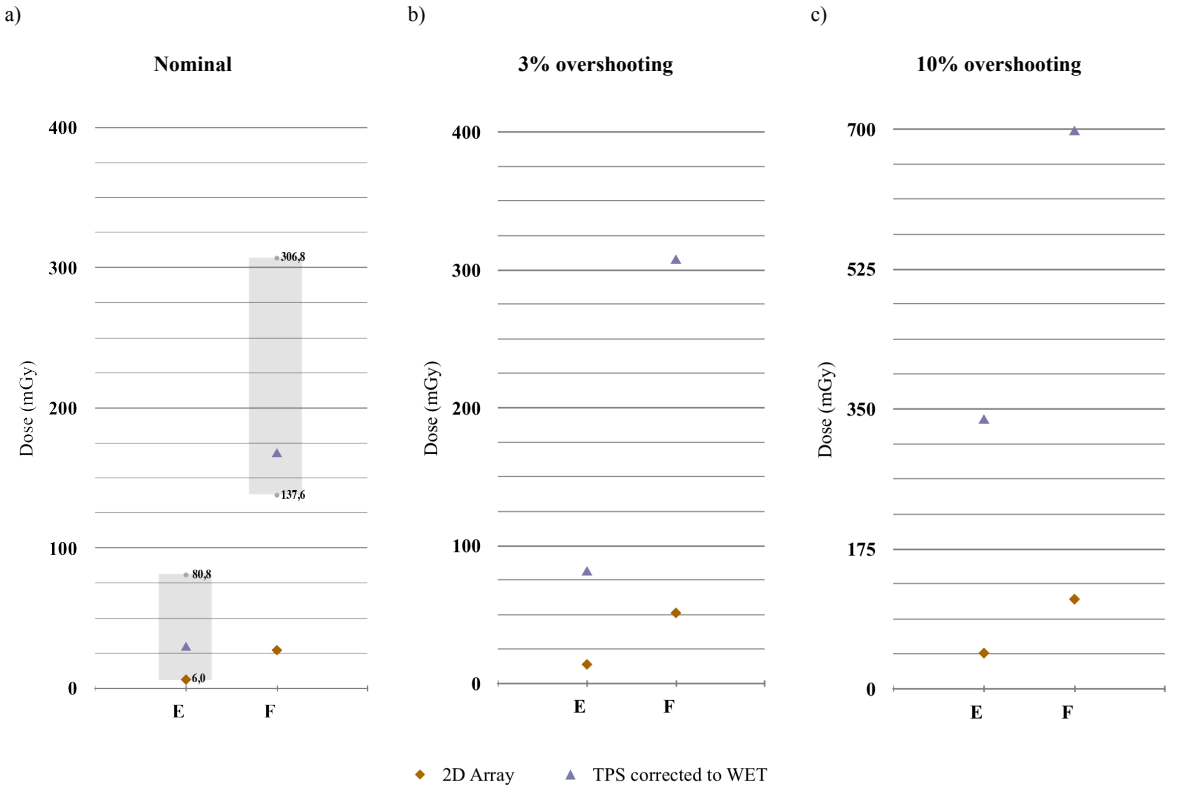

Figure 22: Graphical comparison between TPS prediction results, corrected to the entrance window WET , against the dose actually measured by the 2D array in 2 points: E (R=14, C=14) and F(R=12, C=11) for: a) nominal scenario; b) 3% overshooting scenario; c) 10% overshooting scenario. The dose predicted by the TPS takes into account a RBE value of 1.1.

2D array	TPS
Nominal scenarios	
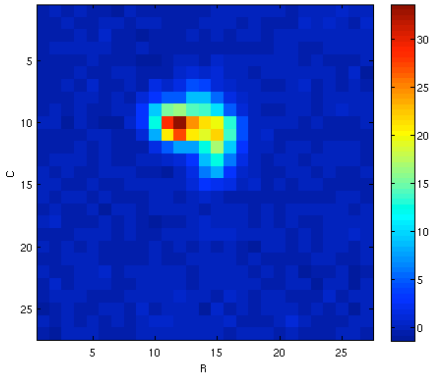	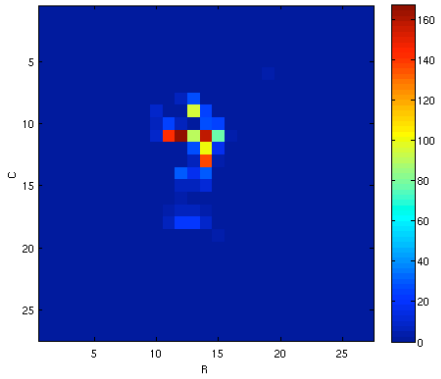
3% overshooting scenarios	
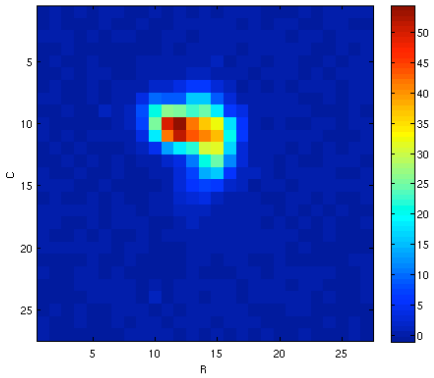	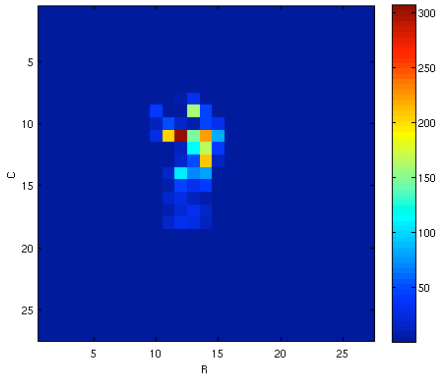
10% overshooting scenarios	
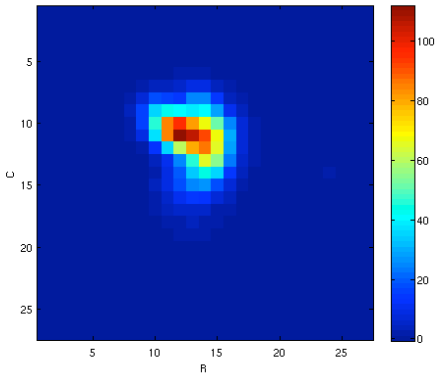	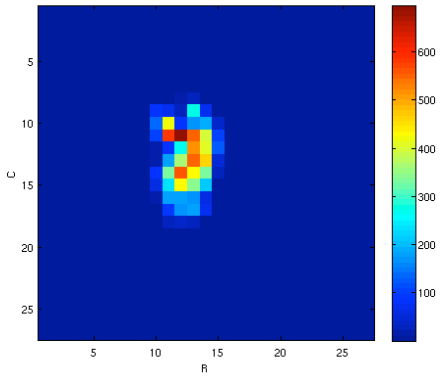

Figure 23: 2D maps resultants of the experimental measurements for all scenarios (left). 2D maps obtained from the pos-processing PTDT file for the 3 scenarios evaluated. The scale values of the 2D array corresponds to Gy. In the TPS the RBE is taking into account (Gy(RBE))

4.2.1.3. Discussion

Despite the position errors have no influence on the uncertainty anymore, the dose predicted is again significantly higher. Again, the relevant character of the heterogeneities existent within the CT can be a significative cause. As explained on the sub-chapter 2.5, the heterogeneities of the patient insert some uncertainty in the range of the beam. In fact the head phantom, being a replica of a patients head, shows a high heterogeneity not only along the beam path but also laterally. There is in fact several abrupt density changes on the CT volume: its evident in the figure 11a several tissue-bones interfaces and even tissue-air interface, due to the nasal cavity. These causes in fact an increase on the MCS uncertainties factor which in the skull can lead to a significant reduction of the beam range. Consequently the dose measured is lesser and the dose distribution more heterogeneous.

In fact, it can be verified a dose difference between the dose predicted by the TPS and the dose measured, as result of the ±3% of uncertainty in the range that actually exists in all the measurements performed, regardless of the scenario. However, the range uncertainties itself do not explain this whole dose difference, as it is verified by the grey areas in figure 22a. The fact that the dose measured is not within the grey area, shows that another error which is not contemplated within the causes of uncertainties in the range was made. Specifically, an error regarding the project procedure.

As described the position errors no longer have an effect. Additionally, the entrance window, which was manually simulated, is then a possible source of error caused by the WET theoretical approximation method applied on its creation. In contrast, a CT image of the 2D array together with the head phantom would probably be a more accurate approximation, however, it would be neither practically or easily to perform.

Finally, it is known that there are still a slightly error in the calculation of the dose in air by the PSIplan. This error is actually corrected concerning the air gap between the nozzle and the patient but between the patient and the 2D array, the error still stands. This could have been a major source of the discrepancies between the dose measured and the dose predicted by the TPS. This not seem to be the case anyway, since the dose was also calculated in a CT where this air gap was removed but the results did not have a relevant improvement.

4.2.2. Point detectors over the 2D array

Point detectors were also used to reproduce the measurements in the specified points chosen to evaluate the dose: point E and F. Four different detectors were used and for each one the dose in each point was measured 3 times. Despite the 10% overshooting had been created specially for the 2D array, this scenario was as well evaluated in these point detector measurements. The results obtained are listed in the following table 5 and in the graphics of figure 24.

	IC Semiflex (mGy)	IC A. Markus (mGy)	Diamond detector (mGy)	TLD (mGy)	TPS (mGy(RBE))
E (R=14,C=14)					
nominal	51.2 (5.6%)	63.1 (6.9%)	39.5 (4.3%)	49.3 (5.4%)	195.4 (21.5%)
overshooting 3%	99.2 (11%)	117.0 (12.9%)	84.0 (9.2%)	-	337.0 (37%)
overshooting 10%	184 .0 (20%)	205.6 (22.6 %)	157.7 (17.3%)	190.0 (20.9%)	549.3 (60.4%)
F (R=12, C=11)					
nominal	98.1 (10.8%)	111.0 (12.2%)	-	115.3 (12.7%)	620.2 (68.1%)
overshooting 3%	164.6 (18.1%)	187.1 (20.6%)	-	-	692.9 (76.1%)
overshooting 10%	261.8 (28.8%)	296.4 (32.6%)	-	290.7 (31.9%)	845.7 (92.9%)

Table 5: Results of the method 2 measurements for the dosimeters positioned over the 2D array points: the central IC and for the IC with coordinates (R=12, C=11). The diamond detector was only used in the central point while the TLDs were not use for the 3% overshooting scenario. The percent values correspond to the percentage of dose measured relative to the dose prescribed, 910 mGy(RBE).

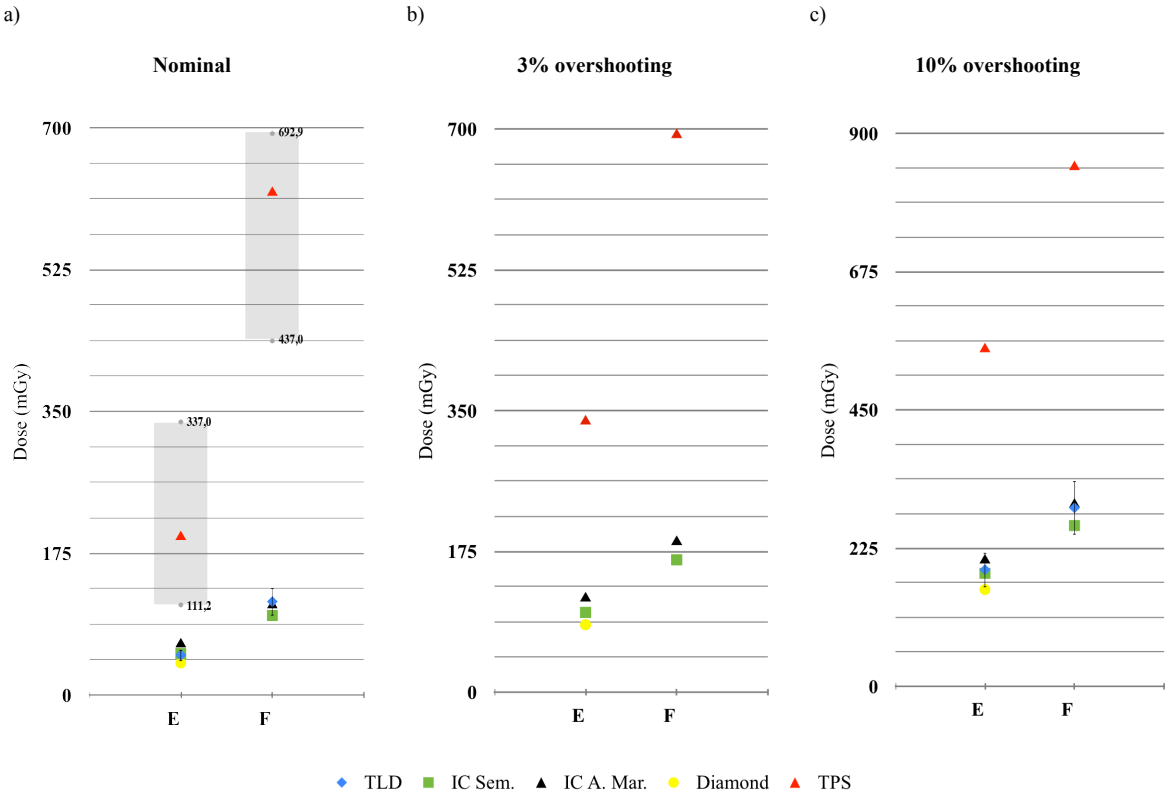

Figure 24: Graphical comparison between TPS prediction results, against the dose actually measured by 4 different detectors placed points: E (R=14, C=14) and F(R=12, C=11) for: a) nominal scenario; b) 3% overshooting scenario; c) 10% overshooting scenario. The dose predicted by the TPS takes into account a RBE value of 1.1.

In order to be easier analyze the results, it is presented in the table 5, along with the dose measured by the detectors or predicted by the TPS, the dose percentage relative to the prescribed dose,

910 mGyRBE. Comparing just the dose measured between the dosimeters, excluding the dose predicted by the PSIplan, one can assume a general agreement. The percentage dose has a variation of ~ ±3% of the prescribed dose between the detectors. On the other hand, the dose predicted by the TPS exceeds substantially the dose measured by all the dosimeters. The graphical representation of the results show these differences (figure 24). Regardless of the scenario, the dose detected agree in general, whilst the TPS dose predicted is around 3 times more than the one measured.

On the other hand, the dose measured is not again within the possible dose variation represented by the grey area bar.

4.2.2.1. Discussion

Comparing the dose measured between the dosimeters, the position errors have again a significant influence. They are one of the causes of the differences that actually are noted, despite the good agreement existent relative to the dose prescribed. Regarding the diamond detector results, it was not placed in it default position, parallel to the beam with the front face perpendicular to it. Instead it was placed laterally to it. This could have influenced the results obtained, which were lower than the ones obtained by the ICs and TLDs.

As a matter of clarification, the TPS values were taken from the PTDT slice corresponding to the position of the detectors (slice x=166) (figure 11b), without the influence of the 2D array entrance window. Taking this into account, one more time it was evident the range uncertainties problem when comparing the dosimeters results with the ones predicted by TPS. Errors inherent to the procedure were committed since the dose measured is not inside the grey area. Although the range uncertainties are inherent to the TPS calculations they do not cover these big differences.

5. Conclusion

It is clear among proton therapy community that the full potential of proton therapy will only be exploited when it will be possible to control and monitor the range uncertainties *in vivo* [2]. Actually, it is notorious the importance of reducing range uncertainties since a small factor that causes a certain uncertainty is translated in a significant dose variation. A precise control would allow the development of more convenient field directions in order to exploit the steeper distal fall-off of proton beams and spare the healthy tissue. In fact, *in vivo* range dosimetry research has been growing and several approaches have been proposed over the last years [2]. The idea of this thesis project arose therefore from this later reality and follow the well establish *in vivo* dosimetry methods for conventional radiotherapy where actually, for instance, TLDs are used for total body irradiation [6].

At the outset, one important issue regarding this EIVD approach is that it only could be used in superficial targets. In targets inside a patient, due to the characteristics of proton beams, the dose would not be measured outside the patient even facing an expressive uncertainty in the range. That was thus the first limitation of the EIVD approach proposed. On the other hand, relative to other methods proposed, the simple clinical methodology, the on-line results and insignificant costs associated, would be an important advantage.

As explained in the methods section, one nominal and two overshooting scenarios were created for the experiments. In fact, after the results evaluation, if only the nominal scenario had been used, the dose could be measured and compared with the dose predicted for the TPS. However, the development of the overshooting scenarios allowed not only the simulation of the effect of +3% error in the range, but also the measurement of a significant amount of dose out of the patient necessary for detectors detection.

Regarding method 1, the results obtained do not allow to take further conclusion about the feasibility of dosimeters for *in vivo* dosimetry. They show the dose predicted by the TPS is in general twice the value of the dose measured. It was verified that, besides the range uncertainties associated to

a treatment (in this case experimental), dosimeter positioning was as well a source of error in the measurements. The dosimeter positioning method used in the experiments, even using the lasers as a support system, is not sufficiently precise. Since the dose was measured in the steep fall-off region of the dose distribution, an high gradient region, the position should have been considerably precise so that the resultant high dose differences were not registered. However, in an eventual EIVD approach, the positioning method precision could not be easily improved.

Contrary to the 2D array entrance window WET, the WET of the dosimeters capsule thickness was not taken into account in TPS calculations. Nevertheless, the simulation of such thickness (around 1 mm for each dosimeter) would not bring relevant differences in the results.

This main problem was then overcome using the 2D array in method 2. On this measurements it was also placed 4 different dosimeters on the surface of the 2D array. Additionally, it was added to the results obtained data obtained from the TPS representing the dose variation caused by a ±3% variation in the proton range (represented in the grey area). This uncertainty is indeed the possible range variation in all treatments performed at PSI. As explained before, the dose measured by the 5 detectors in the nominal scenarios were out of the grey area, i.e, not within the effect of ±3% variation in the range. The overshooting scenario plans, which were used to increase the dose measured in the nominal to significant values, did not bring better results. Therefore, no conclusions about the feasibility of the detectors for the EIVD approach could have been taken. Instead, the results showed that there was an error inherent to the method performed.

Some of this errors in method 2 were in fact taken into account. As mentioned, the simulation in Matlab® of the WET of the 2D array entrance window was needed. It was verified that this simulation had effects in the dose predicted by the TPS, decreasing the dose in the measurement voxels region when compared to the dose in the same region calculated using the original CT, without entrance window simulation[3]. In fact, when measuring experimentally, there is a decrease in the mean proton beam energy, and consequently in the dose measured, due to to the entrance window. Despite this dose decrease, the results obtained and described in the sub-chapter 4.2 did not bring relevant improvements.

Another point that should be referred is the air that exist between the phantom and the 2D array surface. In the experimental measurements, the proton beam path before interact with the 2D array, crosses some centimeters (~20 cm) of air. The effect on the beam resultant of this amount of air is irrelevant, since the stopping power of air compared with the water stopping power is around 800[4] times smaller for the range of proton energies used [36]. In fact, the WET of 20 cm of air is around

3 Results obtained from the original CT were not described in the thesis.

4 Calculations made through the NIST (National Institute of Standards and Technology) PSTAR database .

0,25 mm[5] [37]. However, it is known PSIplan does not calculate the dose in air properly. The TPS corrects this problem in the air gap between the gantry nozzle and the phantom, but behind the phantom, i.e, on the air in the opposite side of the beam nozzle, after the proton beam transverse the phantom, this problem persists. This could be then a source for the TPS overestimation of the results because the 2D array was placed in this air region. In order to try to overcome this problem, other entrance window simulations in Matlab® were performed, however, with no results improvement[6].

Facing this results and consequent impossibility to take conclusions on the feasibility of *in vivo* dosimetry for proton therapy 2 hypothesis can be taken:

- The measurements are being made in an undershooting scenario relative to the TPS, i.e, the TPS is overestimating the range due to uncertainty sources that actually bring a value of range uncertainty bigger than the ±3% used at PSI. However, this is not the reality. One example is the work of Albertini F. et al, where GafChromic films were placed inside the same phantom used in this project, intersecting the target, and the dose was measured through modified dosimetric plans with a CT modification to simulate the range errors (same method used in the project). Results show excellent agreement between the calculated and the measured dose distributions [35]. Then, the results of the project should not characterize or be compared with the dose actually delivered inside the target and specially in a clinical treatment and range uncertainties bigger than ±3% are not the case.

- Since the experimental measurements agree in general within the respective ±3% uncertainty and the position method uncertainty, PSIplan might be indeed overestimating the dose on the opposite side of the gantry nozzle relative to the patient. In fact, incorrect dose in air calculations, although not overcome, are a reality. Other unknown problems that in fact influence the dose predicted in this region by the TPS should not be discarded as well. Due to this problems evidenced by PSIplan and with the goal to reproduce the results obtained by the TPS, a Monte Carlo treatment plan (TOPAS [38]) was used. This is a Monte Carlo simulation tool focused in radiation therapy purposes which has been in beta test phase up to date. At PSI, however, the installation of this software it is not completely finished to date, therefore, the results obtained were not relevant for the project. For future projects, the reproducibility of the TPS could be performed.

This results also corroborate the reason why there are no projects published about a similar EIVD approach, which is widely used in conventional radiotherapy. Even admitting that the sources of uncertainty in the range could be the only cause of range errors between the dose predicted and the one actually measured, this EIVD method would have to be improved concerning the dosimeters positioning. In fact, the steep dose fall-off region, which is the region where the dosimeters would be

[5] Calculations made with the WET formula taken from Zhang R. et al

[6] Since the results obtained with this methods were not relevant, they were not presented in the thesis

placed in such approach, forces a extremely precise positioning. A 3% range error causes for instance a shift of few millimeters (~10 mm), depending on the heterogeneities of the medium (in water the shift is around 8 mm for a 200 MeV proton beam[7]) [36]. Therefore, the uncertainty in the position of dosimeters would have to be a small percentage of this shift in order to obtain relevant information.

An additional note, in case of future similar projects, for the developing of a similar EIVD approach is related with the methodology. In this project, the CT image used was obtained from the phantom head. As referred, it has a high density heterogeneities. Therefore, for instance, a CT representing a water phantom could have been used for the first measurements in order to understand not only the extent of such heterogeneities but also to better analyze the effect of the detector positioning. Finally, regardless of the results obtained, a detector similar to the 2D array but with better spatial resolution, would be a possible solution for this EIVD approach. A dosimeter or method which does not overcome the inherent position errors could indeed never be used for such approach.

[7] Calculated using the PSTAR data base from NIST website

6. Bibliography

1. Ferlay, J., et al., *Cancer incidence and mortality worldwide: sources, methods and major patterns in GLOBOCAN 2012.* Int J Cancer, 2014.

2. Knopf, A.C. and A. Lomax, *In vivo proton range verification: a review.* Phys Med Biol, 2013. **58**(15): p. R131-60.

3. Paganetti, H., *Proton Therapy Physics*2012: CRC Press/Taylor & Francis.

4. Paganetti, H., *Range uncertainties in proton therapy and the role of Monte Carlo simulations.* Phys Med Biol, 2012. **57**(11): p. R99-117.

5. Trofimov, A., et al., *Radiotherapy treatment of early-stage prostate cancer with IMRT and protons: a treatment planning comparison.* Int J Radiat Oncol Biol Phys, 2007. **69**(2): p. 444-53.

6. Mijnheer, B., et al., *In vivo dosimetry in external beam radiotherapy.* Med Phys, 2013. **40**(7): p. 070903.

7. PSI. *Paul Scherrer Institut*. 2014; Available from: http://www.psi.ch/.

8. Mumot, M., et al., *Proton range verification using a range probe: definition of concept and initial analysis.* Phys Med Biol, 2010. **55**(16): p. 4771-82.

9. Lu, H.M., *A potential method for in vivo range verification in proton therapy treatment.* Phys Med Biol, 2008. **53**(5): p. 1413-24.

10. Schneider, U. and E. Pedroni, *Proton radiography as a tool for quality control in proton therapy.* Med Phys, 1995. **22**(4): p. 353-63.

11. Min, C.-H., et al., *Prompt gamma measurements for locating the dose falloff region in the proton therapy.* Applied Physics Letters, 2006. **89**(18): p. -.

12. Kurosawa, S., et al., *Prompt gamma detection for range verification in proton therapy.* Current Applied Physics, 2012. **12**(2): p. 364-368.

13. Paans, A.M.J. and J.M. Schippers, *Proton therapy in combination with PET as monitor: a feasibility study.* Nuclear Science, IEEE Transactions on, 1993. **40**(4): p. 1041-1044.

14. Litzenberg, D.W., et al., *On-line monitoring of radiotherapy beams: experimental results with proton beams.* Med Phys, 1999. **26**(6): p. 992-1006.

15. Vynckier, S., et al., *Is it possible to verify directly a proton-treatment plan using positron emission tomography?* Radiother Oncol, 1993. **26**(3): p. 275-7.

16. Oelfke, U., G.K. Lam, and M.S. Atkins, *Proton dose monitoring with PET: quantitative studies in Lucite.* Phys Med Biol, 1996. **41**(1): p. 177-96.

17. Studenski, M.T. and Y. Xiao, *Proton therapy dosimetry using positron emission tomography.* World J Radiol, 2010. **2**(4): p. 135-42.

18. Parodi, K., et al., *Patient study of in vivo verification of beam delivery and range, using positron emission tomography and computed tomography imaging after proton therapy.* Int J Radiat Oncol Biol Phys, 2007. **68**(3): p. 920-34.

19. Gensheimer, M.F., et al., *In vivo proton beam range verification using spine MRI changes.* Int J Radiat Oncol Biol Phys, 2010. **78**(1): p. 268-75.

20. Goitein, M., *Radiation Oncology: A Physicist's-Eye View: A Physicist's-eye View*2007: Springer.

21. Turner, J.E., *Atoms, radiation, and radiation protection*. 3rd completely rev. and enlarged ed. ed2007, Weinheim: Wiley-VCH ; [Chichester : John Wiley, distributor].

22. International Commission on Radiation, U. and Measurements, *Report 85: Fundamental quantities and units for ionizing radiation.* J ICRU, 2011. **11**(1): p. 1-31.

23. Goitein, M., A. Lomax, and E. Pedroni, *Treating cancer with protons.* Physics Today, 2002 (55): p. 45-50.

24. Albertini, F., *Planning and optimizing treatment plans for actively scanned proton therapy. Evaluating and estimating the effect of uncertainties*, in *Physics department*2011, ETH: Zurich. p. Nr. 19525.

25. Pedroni, E., et al., *The PSI Gantry 2: a second generation proton scanning gantry.* Z Med Phys, 2004. **14**(1): p. 25-34.

26. Zenklusen, S.M., E. Pedroni, and D. Meer, *A study on repainting strategies for treating moderately moving targets with proton pencil beam scanning at the new Gantry 2 at PSI.* Phys Med Biol, 2010. **55**(17): p. 5103-21.

27. Suetens, P., *Fundamentals of Medical Imaging*2009: Cambridge University Press.

28. Schneider, U., E. Pedroni, and A. Lomax, *The calibration of CT Hounsfield units for radiotherapy treatment planning.* Phys Med Biol, 1996. **41**(1): p. 111-24.

29. Podgoršak, E.B. and I.A.E. Agency, *Radiation oncology physics: a handbook for teachers and students*2005: International Atomic Energy Agency.

30. PTW, *Ionizing Radiation - Detectors*, in *Radiation Therapy*, PTW, Editor 2014.

31. Mandapaka, A.K., et al., *Evaluation of the dosimetric properties of a synthetic single crystal diamond detector in high energy clinical proton beams.* Medical Physics, 2013. **40**(12): p. -.

32. PTW, *microDiamond - Synthetic Diamond Detector for High-Precision Dosimetry*, in *Detectors*, PTW, Editor 2014.

33. Spezi, E., et al., *Characterization of a 2D ion chamber array for the verification of radiotherapy treatments.* Phys Med Biol, 2005. **50**(14): p. 3361-73.

34. Agency, I.A.E., *Absorbed dose determination in external beam radiotherapy: an international code of practice for dosimetry based on standards of absorbed dose to water*2000: International Atomic Energy Agency.

35. Albertini, F., et al., *Experimental verification of IMPT treatment plans in an anthropomorphic phantom in the presence of delivery uncertainties.* Phys Med Biol, 2011. **56**(14): p. 4415-31.

36. NIST. *National Institute of Standards and Technology (NIST)*. 2010; Available from: http://physics.nist.gov/PhysRefData/Star/Text/PSTAR.html.

37. Zhang, R. and W.D. Newhauser, *Calculation of water equivalent thickness of materials of arbitrary density, elemental composition and thickness in proton beam irradiation.* Phys Med Biol, 2009. **54**(6): p. 1383-95.

38. Perl, J., et al., *TOPAS: an innovative proton Monte Carlo platform for research and clinical applications.* Med Phys, 2012. **39**(11): p. 6818-37.

39. Safai, S., *Development of a Dosimetric Phantom with 400 pointlike Scintillators coupled to Optical Light Guides for 3D Verification Dosimetry for Scanned Proton Beam*, in *Physics department*2005, Swiss federal institut of thecnology: Zurich.

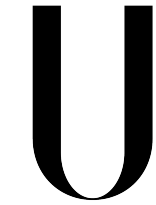

LISBOA

UNIVERSIDADE
DE LISBOA